MATERIALS CHEMISTRY FRONTIERS

REVIEW

View Article Online
View Journal | View Issue

Cite this: *Mater. Chem. Front.*, 2025, **9**, 3096

Organic–inorganic hybrid halide perovskites for field-effect transistors

Sichen Liu,[a] Xuanxuan Sun,[a] Tianbo Zheng,[a] Qinghua Xu,*[b] Yao Gao*[a] and Xing Lu*[a]

Organic–inorganic hybrid halide perovskites exhibit exceptional properties, including prolonged charge carrier lifetimes, high photoluminescence quantum efficiency, and remarkable defect tolerance, demonstrating significant potential in optoelectronic applications like photoelectric detectors, light-emitting devices, and solar cells. Despite the high intrinsic carrier mobilities, their application in field-effect transistors (FETs) has not been well investigated. Three critical challenges currently hinder the development of high-performance hybrid halide perovskite FETs: ion migration, bulk/interfacial defects, and material instability. In the past few years, the application of halide perovskites as FET channel materials has been actively advancing, not only for the development of high-performance FETs showing stunningly improved mobilities, but also for fundamental investigation of charge transport mechanisms and structure–property relationships. This article comprehensively reviews recent progress in three-dimensional (3D) and two-dimensional (2D) organic–inorganic hybrid halide perovskite-based FETs. We discuss achievements and current challenges regarding device performance and stability issues of such hybrid materials and provide a general perspective on breaking through their bottlenecks and exploring future directions.

Received 17th May 2025,
Accepted 3rd September 2025

DOI: 10.1039/d5qm00380f

rsc.li/frontiers-materials

[a] *State Key Laboratory of Materials Processing and Die & Mould Technology, School of Materials Science and Engineering, Huazhong University of Science and Technology, Wuhan 430074, China. E-mail: yaogao@hust.edu.cn, lux@hust.edu.cn*

[b] *School of Pharmaceutical Sciences, South-Central Minzu University, Wuhan 430074, China. E-mail: 2023143@mail.scuec.edu.cn*

Sichen Liu

Sichen Liu is currently a PhD student in the School of Materials Science and Engineering, Huazhong University of Science and Technology. She obtained her BS in Environmental Science from Shenyang Pharmaceutical University in 2020. She then obtained an engineering master's degree under the supervision of Prof. Guanben Du and Prof. Long Yang at the School of Materials Chemistry and Engineering, Southwest Forestry University from 2020 to 2023. She started pursuing her PhD degree and joined Prof. Xing Lu and Yao Gao's groups in 2023. Her current research focuses on synthesizing organic–inorganic hybrid halide perovskites and their applications in FETs.

Xuanxuan Sun

Xuanxuan Sun obtained a Bachelor's degree in Materials Science and Engineering from the University of Shanghai for Science and Technology in 2018. From 2022 to 2025, she studied at the School of Materials Science and Engineering, Huazhong University of Science and Technology, pursuing a Master's degree in the research group of Professor Lu Xing. Her research interests include design and synthesis of new conjugated organic ligands, which are used in two-dimensional organic–inorganic hybrid perovskite materials and applied to FET devices.

1. Introduction to hybrid halide perovskites and processing of perovskite FETs

Organic–inorganic hybrid halide perovskites have distinguished themselves in emerging optoelectronic applications due to their excellent properties such as a high optical absorption coefficient, adjustable band gap, long carrier diffusion constant, low exciton binding energy and solution processing properties, and the performance records continue to be broken in solar cells, light-emitting diodes, photodetectors, lasers, transistors, and more. The chemical formula of three-dimensional (3D) metal halide perovskites (MHPs) is generally ABX_3, where A stands for a monovalent ion, such as inorganic Cs^+ or Ru^+, or organic cations like methylammonium (MA^+) or formamidinium (FA^+), B represents a divalent metal cation (*e.g.*, Pb^{2+} and Sn^{2+}), and X represents halogen anions (*e.g.*, Cl^-, Br^-, and I^-). Based on this, the B and X ions form inorganic $[BX_6]^{4-}$ octahedra (the B ions at the center of the octahedra and the X ions at the corner) which are arranged three-dimensionally by sharing the octahedral corners, with the A cations filling the gaps between the octahedral units,[1,2] as shown in Fig. 1a. It's worth noting that the layered structure of perovskites can be obtained by using bulk organic ammonium

Tianbo Zheng

Tianbo Zheng is a first-year PhD student at the School of Materials Science and Engineering, Huazhong University of Science and Technology. Her research focuses on the structural design and synthesis of conjugated organic ligands to develop two-dimensional organic–inorganic hybrid perovskites for optoelectronic applications.

Qinghua Xu

Dr Qinghua Xu received her PhD degree in Polymer Chemistry from the Changchun Institute of Applied Chemistry, University of Chinese Academy of Sciences in 2017. She then worked as a postdoctoral researcher from 2017 to 2020 at Cornell University and from 2020 to 2022 at Purdue University. She is an associate professor of Pharmaceutical Preparation at the School of Pharmaceutical Sciences, South-central Minzu University. Her research interests include synthetic and natural polymer-based nanoparticles and hydrogels for drug delivery, tissue engineering and bioimaging.

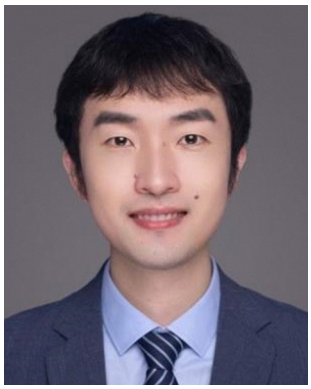

Yao Gao

Prof. Yao Gao joined the School of Materials Science and Engineering, Huazhong University of Science and Technology in 2022. He obtained BS in Chemistry from Nanjing University in 2011 and PhD in Polymer Chemistry and Physics from the Changchun Institute of Applied Chemistry, Chinese Academy of Sciences in 2017. From 2017 to 2021, he was a postdoctoral fellow at the Davidson School of Chemical Engineering of Purdue University. His research interest includes the synthesis and characterization of organic and hybrid semiconducting materials, fundamental understanding of their structure–property relationships, as well as their applications in optoelectronic devices.

Xing Lu

Xing Lu is currently a professor in Hainan University and an Adjunct Professor in the Huazhong University of Science and Technology. He received his BS, MS and PhD from Xiamen University (1998), the Changchun Institute of Applied Chemistry, Chinese Academy of Sciences (2001) and Peking University (2004), respectively. Then he worked as a COE Postdoctoral researcher in Nagoya University, Japan. From 2006 to 2013, he was a Senior Scientist in the University of Tsukuba, Japan. He is the recipient of The Ambassador Award from Chinese Embassy in Japan (2009), The Osawa Award from Fullerenes and Nanotubes Research Society of Japan (2011) and The National Science Fund for Distinguished Young Scholars (2019). His research interests lie in the rational design and facile generation of novel hybrid carbon materials with applications in energy storage and conversion. He has published more than 200 peer-reviewed papers in international journals with >60 at Nat. Syn., Nat. Commun., J. Am. Chem. Soc., Angew. Chem., Int. Ed. and so on.

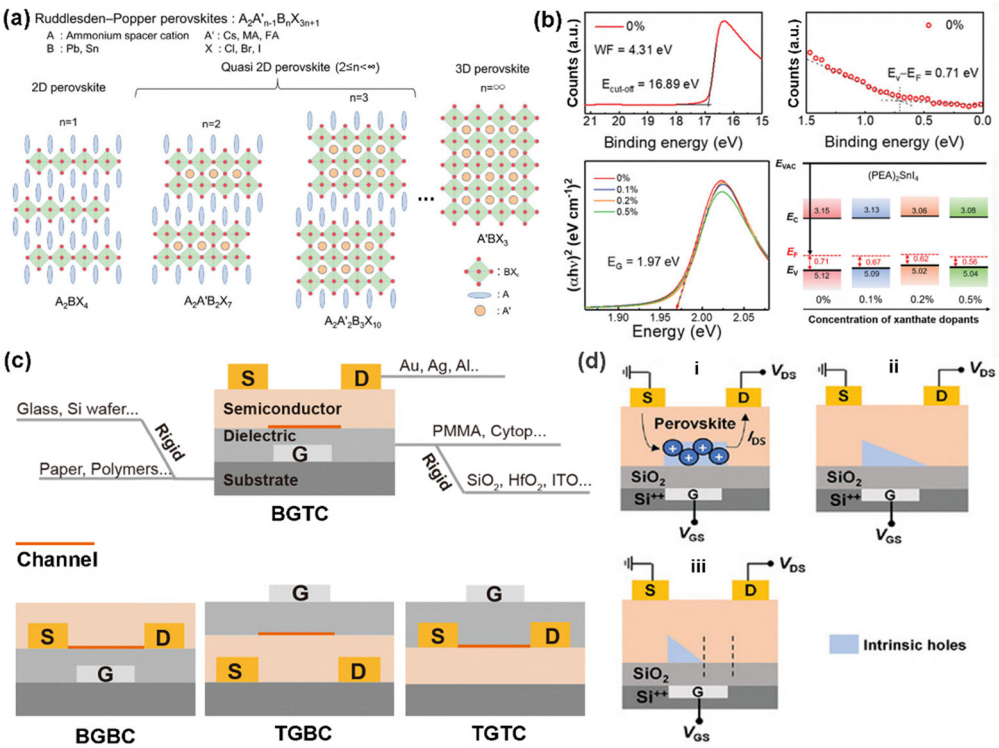

Fig. 1 (a) Schematic of crystal structures for 2D, quasi-2D, and 3D metal halide perovskites.[23] (b) Determination of work function, valence band maximum (VBM), and conduction band minimum (CBM) *via* ultraviolet photoelectron spectroscopy (UPS).[10] (c) Schematic cross-sections for four general organic transistor geometries: bottom gate top contact (BGTC), bottom gate bottom contact (BGBC), top gate bottom contact (TGBC), and top gate top contact (TGTC). (d) Illustrations of operating regimes of FETs, (i), (ii), and (iii), represent the linear regime, the start of the saturation regime at the pinch-off point, and the saturation regime, respectively.[7] Figures reproduced with permission from: (a) ref. 23. Copyright 2021, Wiley-VCH GmbH; (b) ref. 10. Copyright 2022, Wiley-VCH GmbH; (d) ref. 7.

cations (such as butylammonium and phenylethylammonium) as A-site ions. The general structure formula is $A'_2A_{n-1}M_nX_{3n+1}$ (A′ is +1) or $A''A_{n-1}M_nX_{3n+1}$ (A″ is +2), where n represents the number of inorganic $[BX_6]^{4-}$ layers, and 2D and quasi-2D perovskite structures can be obtained by adjusting the n value.[3] Theoretically, the n of 3D perovskites is ∞. In 2D perovskites, one of the two A-site cations needs to be large enough to separate the inorganic layer and the other should be small enough to fill the octahedral gap.[2]

In addition to the crystal structure, the band structure is also important for understanding and studying perovskites. Among the components that constitute the structure of perovskite crystals, the A-site cation primarily influences the crystal structure by modifying the lattice. Since it does not participate in covalent bonding, its impact on the frontier energy bands is minimal.[4] Therefore, the energy density of perovskite semiconductors is mainly provided by the electron cloud distribution of the valence electron layer of B-site metals and halogens. For the commonly used Pb/Sn-based perovskites (inorganic parts are $[PbI_6]^{4-}$ and $[SnI_6]^{4-}$), the origin of the valence band (VB) is the anti-bonding of the Sn/Pb-s orbitals and I-5p orbitals, and the dominant origin of the conduction band (CB) is Sn/Pb-p orbitals.[4,5] In particular, Sn-5s and Sn-5p orbitals are higher than Pb-6s and Pb-6p orbitals, so Sn-based perovskites have strong Sn 5s–I 5p anti-bonding coupling, which not only improves the energy level of the VB, but also reduces the band gap.[6] The strong anti-bonding coupling promotes the formation of tin vacancies (V_{Sn}), which are the source of the holes, so Sn-based perovskites exhibit more p-type characteristics.[7] However, too many V_{Sn} can induce a p-type self-doping effect that has a negative influence on the performance of the FET device.[8]

So far, there have been numerous methods to characterize the band structure, such as ultraviolet photoelectron spectroscopy (UPS), ultraviolet-visible absorption spectroscopy (UV-vis), UV-vis diffuse reflectance spectroscopy, X-ray photoelectron spectroscopy (XPS), cyclic voltammetry (CV), and density functional theory (DFT) calculation.[9–11] In general, these methods are convenient to use in combination. Taking $(PEA)_2SnI_4$ in Fig. 1b as an example, firstly, the intersection of the intensity at a high binding energy in UPS is defined as the secondary electron cutoff energy ($E_{cut-off}$); the work function can be determined by the difference between the incident photon energy and $E_{cut-off}$; and the intersection of the intensity at the low binding energy represents the difference between the valence band energy and the Fermi energy level ($E_v - E_F$). E_v can be gained by the intersection of the epitaxial line near 0 eV and the horizontal extension in the XPS valence band spectrum. Next, the E_g is estimated according to the Tauc plot, which is mainly based on the formula: $(\alpha h\nu)^{1/n} = B(h\nu - E_g)$ (n = 1/2 for

the direct bandgap, $n = 2$ for the indirect bandgap). From the above formula, it can be seen that $(\alpha h\nu)^{1/n}$ is only linear with $h\nu$, so the tangent of the extension curve intersects the *X*-axis, and the E_g of the semiconductor material can be obtained. Also, the band edge absorption wavelength (λ_g) of the semiconductor is determined by the band gap width E_g, and there is a quantitative relationship between them: $E_g = 1240/\lambda_g$. Then the E_g can be obtained using the UV-vis spectrum, but this method is only suitable for direct band gap semiconductors. Finally, E_c is obtained by converting E_g and E_v. The energy band diagram of $(PEA)_2SnI_4$ can be determined by combining E_c, E_v, and E_F. The diagrams show that after replacing partly V_I^+ by S^{2-} doping, the Fermi level is closer to VBM, indicating that the hole concentration increases (Fig. 1b). The CV method is used widely to estimate ionization energy IP (or the HOMO) and electron affinity energy EA (or the LUMO) by measuring redox potential. The initial oxidation potential corresponds approximately to IP. The initial reduction potential corresponds to EA. The difference between the two corresponds to the E_g of the semiconductor.

MHPs have advantages in electron transport, large-area deposition at low temperatures, high carrier mobility, and photoelectric conversion, which fully meet the needs of high-performance FET development. However, the application of field-effect transistors was far less popular than that of other optoelectronic devices, until the last two decades have slowly ushered in a renaissance. Field-effect transistors are electronic switches controlled by a voltage circuit, and are the key component of modern electronic technology due to high input impedance, low power consumption, and fast switching speeds. It has been widely used in various electronic products, and its development and application are of great significance for technological innovations and social progress. Generally, apart from their ability to amplify signals and achieve fast switching, the FETs also offer the advantage of low noise, as charge transport involves only a single type of carrier (electrons or holes).[9] The basic structure of a FET usually consists of a substrate, source electrode, drain electrode, gate electrode, dielectric layer, and semiconductor active layer. The semiconductor layer directly contacts the source and drain terminals to form a channel, and the gate terminal is close to the channel but separated by a thin dielectric layer. According to the position of the deposited gate and the contact mode between the semiconductor and the electrode, the device structure is generally divided into bottom-gate and top-contact (BGTC), bottom-gate and bottom-contact (BGBC), top-gate and bottom-contact (TGBC), and top-gate and top-contact (TGTC). The difference in the structure will affect the carrier injection and device performance. Schematic cross-sections for four transistor geometries are shown in Fig. 1c. The BGTC structure with staggered configurations is commonly used in device fabrication, which can lead to better electrical contact because of the large charge injection area and a slight mixing between electrodes and semiconductors, such as Au and $(PEA)_2SnI_4$. However, transistor performance is susceptible to negative effects due to the existence of bulk resistance on the path between the Au electrodes and the channel in the BGTC structure. This phenomenon is more obvious in layered organic–inorganic perovskites, because the vertical transport of the carriers injected from the source to the dielectric interface needs to pass through the quantum well structure between the smaller-bandgap inorganic and larger-bandgap organic sheets under transistor operation.[12,13] There are some solutions to reduce the bulk resistance, including the decrease of semiconductor thickness (t) and increase of channel length (L).[14]

Highly doped silicon wafers serving as substrates and gate electrodes simultaneously are most commonly used in the preparation of high-quality FET devices, and the SiO_2 layer is formed on the Si substrate surface by a high-temperature (900–1200 °C) oxidation reaction.[15] Nevertheless, due to its low dielectric constant, thinner SiO_2 (less than 10 nm) can cause the penetration of charge carriers and lead to high gate leakage current, thus limiting the development of miniaturized devices. Studies have shown that the proper integration of vdW heterojunctions in the device seems to offer an opportunity to improve device performance in short-channel FETs, as a clean van der Waals (vdW) gap is an effective tunneling barrier that reduces the probability of carrier tunneling and thus inhibits gate leakage current.[16] In addition, a heterojunction also facilitates hole transfer and improves device performance.[17] Another limitation of the silicon wafers is their rigidity, which restricts the development of flexible devices.[18] Thus, the substrate to be selected can be rigid (such as ITO glass and bare glass) or flexible (such as plastic, polymers, and paper) according to the requirement of the actual application, and it is the same for the insulation layer. Poly(methyl methacrylate) (PMMA) has been introduced into perovskite transistors as a dielectric because it can overcome the non-orthogonality issues between the perovskite solvent processing and the underlying polymers, be processed at low temperature, and has some negligible –OH groups that can help trap carriers.[19,20] Poly(perfluorobutenylvinylether) (Cytop) with low surface energy induces poor wettability for any solution-processed semiconductor thin films, so it is often used as a dielectric material in a top-gate layout.[20] Of course, adjusting the surface wettability of Cytop by surface treatment will be beneficial for subsequent solution processing.[21] Metals that match the work function of the active channel are normally selected for the materials of source and drain electrodes, for example, Au, Ag, Al, *etc.* The semiconductor layer is the core component that determines the conductivity of FETs. The thickness should not exceed 100 nm since excessive thickness is not conducive to the vertical transport of carriers.[22] Inorganic silicon, transition metal oxides, organic polymers, and perovskite materials have been booming in the field of FETs in recent years. Table 1 summarizes and compares these four mainstream semiconductor materials in terms of mobility, stability, processability, and flexibility. Among them, halide perovskites also take advantage of low cost, easy manufacturing, long carrier diffusion length, low defect density, high carrier mobility, strong PL intensity, *etc.*, and are suitable for the active layer of FETs. This is also the focus of this article and will be discussed in detail below.

Table 1 Summary of the advantages and limitations of inorganic silicon, transition metal oxides, organic polymers and halide perovskite in field-effect transistors

Materials	Advantages	Limitations	Ref.
Inorganic silicon	High mobility Extreme stability Mature technolygy	Rigid Opaque High cost	15 and 24
Transition metal oxides	Medium mobility Good stablibity Transparent	Scarcity of ingradients (such as indium)	24–26
Organic polymers	Excellent flexibility Low processing cost Suitable for printing	Low mobility Poor stability	27 and 28
Halide perovskite	High mobility Low processing cost	Poor stability Toxic (Pb)	29 and 30

2. Working mechanism of perovskite FETs

The operating mechanism of FETs commonly involves the following physical processes: applying a gate voltage (V_g) creates an electric potential between the source and drain electrodes to form a conductive channel; carriers are injected and aggregated into the channel under an electric field; applying a drain voltage (V_d) generates an electric potential to drive the aggregated carriers from the source to the drain electrode, including vertical and horizontal charge carrier transport.[31] When V_g and V_d are applied simultaneously, a controlled current will be formed between the source and the drain electrodes, and basic operating regimes are illustrated in Fig. 1d. Some basic conditions are explained: (1) the positive V_g will induce the injection of negative charges (electrons) at the dielectric/semiconductor interface, and the negative V_g leads to the accumulation of positive charge (holes); (2) the amount of charge accumulated in the channel is proportional to the gate voltage and the capacitance (C_i) of the insulator; (3) the induced charge generated by the applied voltage needs to fill the deep traps at the interface before it can move freely, in other words, the applied V_g must be higher than the threshold voltage (V_{th}), so the effective V_g is $V_g - V_{th}$.[18,24] The channel potential at the source and the drain is 0 and V_{ds}, respectively. If only the V_g is applied, there will be no source–drain bias (V_{ds}), and the potential difference $V_{(x)}$ at the source and the drain will be the same, indicating that the carrier concentrations in the channel are uniform. When a small V_{ds} is applied ($V_{ds} \ll V_g - V_{th}$, Fig. 1d-i), a linear gradient relationship of the charge density will form from source injection to drain extraction. This phase is called the linear regime of FETs, and the source–drain current (I_d) in this region increases linearly with the increase of V_{ds}. As the V_{ds} continues to increase and reaches a point of $V_{ds} = V_g - V_{th}$, the $V_{(x)}$ at the drain declines to 0, at which the channel is ''pinched off'' (Fig. 1d-ii). At the same time, a carrier depletion zone is created in the channel, and the difference between the local potential $V_{(x)}$ and the V_g is below V_{th}, which means that there is not enough electric field to drive the extra carriers to the drain. In the depletion region, a space-charge-limited saturation current $I_{d,sat}$ still can flow across the narrow depletion zone under a relatively high electric field force. Furthermore, the V_{ds} increases continuously ($V_{ds} > V_g - V_{th}$, Fig. 1d-iii), and the depletion zone will be lengthened and the channel will be shortened slightly. The I_d remains unchanged as the V_{ds} increases due to the existence of the depletion zone, and the working region is called the saturation region.

The working regime can be reflected in the volt–ampere (I–V) characteristic curve to better understand the working mechanism of FETs. As shown in Fig. 2a-i, the curve of I_d changes with V_{ds} at a certain gate voltage is called the output characteristic curve. The I_d changes linearly when V_{ds} is small and remains constant at a large bias. When the device is at the point of pinch-off, the output characteristics appear as the inflection point between the linear region and the saturated region. As displayed in Fig. 2a-ii and iii, the curve in which I_d varies with V_g under an unaltered V_{ds} is defined as a transfer characteristic curve. The two figures show the transfer characteristic of the linear region and the saturated region respectively, during device operation. Important performance parameters, including field-effect mobility (μ), the ratio of I_{on}/I_{off}, threshold voltage (V_{th}), and subthreshold swing (SS), can be calculated based on output/transfer characteristic curves. The μ is mainly used to evaluate the carrier transmission speed, which determines the switching response speed of the device and can be extracted from the transfer characteristic curve. For the linear region, the formula $\mu_{lin} = \frac{L}{W \times C_i \times V_{ds}} \times \frac{\partial I_d}{\partial V_g}$ is used, where L is the channel length that is the distance between source and drain electrodes, W is the channel width that is the width of the source and drain electrodes, and C_i is the capacitance of the gate-channel. For the saturation region, the μ_{sat} is independent of V_{ds} and can be gained *via* the formula $\mu_{sat} = \frac{2L}{W \times C_i} \times \left(\frac{\partial \sqrt{I_d}}{\partial V_g}\right)^2$. I_{on}/I_{off} is the ratio of the drain current of FETs in the on-state and the off-state, which reflects the switching performance of the device under a particular gate voltage. A high I_{on}/I_{off} means higher stability, anti-interference ability, and driveability, so a higher value is desirable. The threshold voltage is the minimum voltage required for a semiconductor to form a conducting channel. The V_{th} is the intersection ($I_d = 0$) of the linear part of the linear transfer characteristic curve that extends to the horizontal coordinate of V_g. The V_{th} in the saturation region is obtained

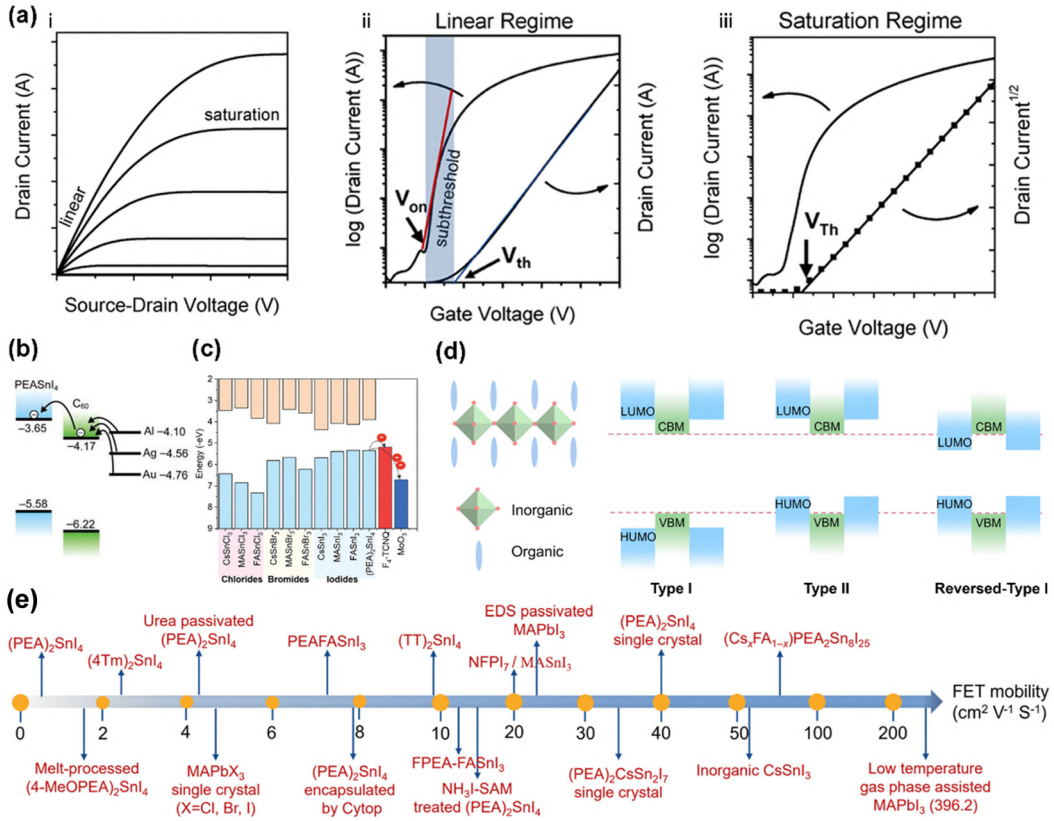

Fig. 2 (a) Representative current–voltage characteristics of an n-channel FET: (i) shows output characteristics curves; (ii) shows transfer characteristics in the linear regime, indicating the onset voltage (V_{on}) when the drain current increases abruptly; (iii) shows transfer characteristics in the saturation regime, indicating the threshold voltage (V_{th}), where the linear fit to the square root of the drain current intersects with the x-axis.[32] (b) Energy-level diagram showing electron injection from the metal electrode (Al, Ag, and Au) to $(PEA)_2SnI_4$ *via* C_{60}.[34] (c) Schematic of the energy levels in different Sn-based perovskites and electron transfer process from $(PEA)_2SnI_4$ to the molecular dopants (p-doping).[7] Figures reproduced with permission from: (a) ref. 32. Copyright 2007, American Chemical Society; (b) ref. 34; (c) ref. 7. (d) Scheme of the 2D perovskite structure (n = 1) and quantum wells with type I, type II, and reversed type I energy alignment. (e) Development roadmap of representative perovskite FET mobility based on different types of halide perovskite.

from the $I_d^{1/2}$–V_g curve using the same method as above. SS indicates the switching ability between the device's on and off states. For the extraction of the SS, firstly, the I_d–V_g curve is log-processed to obtain the semi-log plot ($\log I_d$–V_g). Then, the corresponding onset voltage (V_{on}), when the I_d increases significantly, is found as the starting point of the subthreshold region, and the V_{th} is the endpoint. Next, the semi-log plot in the subthreshold region is fitted linearly, and the reciprocal of the slope ($dV_g/d(\log I_d)$) is SS. In conclusion, an excellent FET device should have a high mobility, a high I_{on}/I_{off}, a low operating voltage, a small subthreshold swing, high stability, and high consistency.

During the operation of perovskite FETs, charge carriers are transported through the inorganic octahedra. However, the energy band edge of perovskites and the Fermi level of the source/drain materials make it difficult to maintain unity, so the existence of an injection barrier makes carrier injection tough.[12] For an organic–inorganic hybrid perovskite, electrons (n-channel FETs) or holes (p-channel FETs) also need to be injected into the band edges. Similarly, if the work function of the electrode metal is not consistent with the band edges, an injection barrier and non-ohmic contact can be introduced.[32] Compared with the coplanar geometry of BGBC and TGTC, TGBC and BGTC have an interleaved geometry, so the source and drain overlap with the gate, which can provide a larger charge injection area. Other efforts have been focused on taking electrode materials with low work function or inserting carrier injection layers between electrodes and semiconductors to reduce the injection barrier.[33] The LUMO level of C_{60} is −4.17 eV, which is between the CBM of $(PEA)_2SnI_4$ (−3.65 eV) and the E_F of Ag (−4.56 eV) and Au (−4.76 eV), making electron injection easier compared with injection directly from the electrode (Fig. 2b).[34] Alternatively, using low work function Al as the electrode can also relax the injection barrier. The VBM of various Sn-based perovskites with different halogens is compared with the LUMO levels of hole dopants F_4-TCNQ and MoO_3 in Fig. 2c.[7] As the p orbitals of halogens change from iodine and bromine to chlorine, the VBM is correspondingly transferred to lower energy levels. The closer the LUMO level of the dopant is to the VBM of perovskites, the more favorable it is to extract electrons, leaving more holes to fill the trap, thus increasing mobility. In particular, organic spacer cations in the organic–inorganic hybrid perovskites separate the inorganic layers, thus forming a quantum well structure composed of

organic barriers and inorganic wells.[3] As shown in Fig. 2d, in type I, the LUMO and HOMO energy levels of organic components are shallower or deeper than the CBM and VBM, respectively, with very large HOMO–LUMO gaps. By extending the conjugated ligand length, band alignment between organic and inorganic parts can be adjusted to make the quantum well structure appear type II or anti-type I.[11] Based on long-chain conjugated ligands, taking a selenophenol conjugated ligand to replace partly thiophene, which can be conducive to reducing the band gap of the ligand by increasing the HOMO energy level due to selenium having a larger and looser outermost electron cloud, thus can help the improvement of the orbital overlap and charge carrier mobility.[35]

Mobility is one of the main goals of the halide perovskite FET revolution. Fig. 2e summarizes the breakthroughs and representative works in the development process of halide perovskite FETs in the past 20 years. The performance has been greatly improved, and it is just a matter of time before it is on par with champion silicon. In this review, we briefly introduce the device structure, working principle, and performance parameters of FETs; the basic principle of MHPs, including crystal structures and band energy structures. Recent developments of 3D and 2D halide perovskites and the mechanism of temperature and other influencing factors on mobility are reviewed and discussed. Next, the causes of poor FETs' stability of halide perovskites are analyzed, and the strategies to improve the stability are summarized. Finally, new ways and future directions to further improve MHP FET performance are outlined.

3. Three-dimensional halide perovskite FETs

The all-inorganic metal halide perovskite $CsSnI_3$ is equipped with an extremely high hole mobility of $\sim 585\ cm^2\ V^{-1}\ s^{-1}$, and has great potential for the preparation of high-performance p-channel transistors, but few reports have been published.[36] Recently, the all-inorganic p-channel $CsSnI_3$-based FETs with BGTC structures (Fig. 3a-i) optimized by precursor engineering (SnF_2-modified CsI precursor solution) demonstrated a mobility of over 50 $cm^2\ V^{-1}\ s^{-1}$ and an on/off current ratio of over

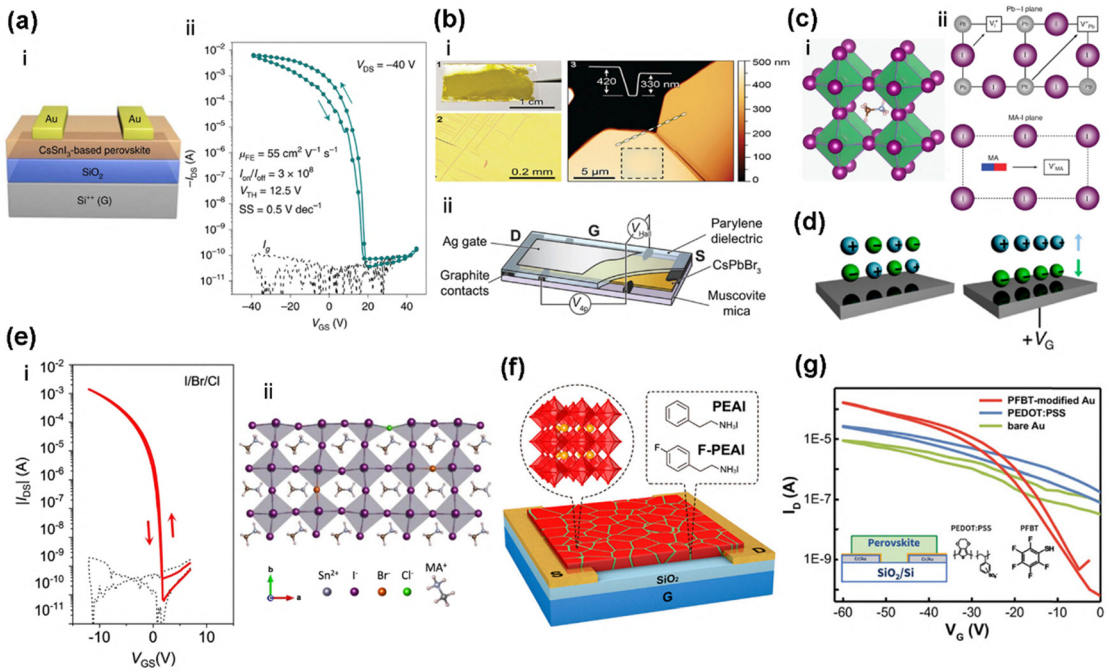

Fig. 3 (a) (i) BGTC TFT structure based on $CsSnI_3$ perovskite. (ii) Transfer characteristics of optimized $CsSnI_3$ (CsI/SnI_2 = 1.25) perovskite channels processed from the Pb-substituted (10 mol%) precursor containing 7 mol% SnF_2 as additive. I_g in (ii) indicates the gate leakage current.[37] Reproduced from ref. 37 with permission from the Springer Nature. (b) (i) Optical photograph (1), optical microscopy image (2), and AFM topography image (3) of large-area epitaxial single-crystal $CsPbBr_3$ thin films. (ii) A sketch of the coplanar TCTG FET structure with large-area epitaxial single-crystal $CsPbBr_3$ thin films as a channel.[41] Reproduced from ref. 41 with permission from the Wiley-VCH GmbH. (c) Transport mechanisms (ii) in the $CH_3NH_3PbI_3$ perovskite structure (which is depicted in (i).[47] Reproduced from ref. 47 with permission from the Springer Nature. (d) Schematic representation of the proposed polarization mechanism of mobile ionic species in $CH_3NH_3PbI_3$ perovskite, under the influence of the external applied gate field (V_G).[51] Reproduced from ref. 51 with permission from the American Chemical Society. (e) (i) Transfer characteristics of the TFTs with $MASnX_3$ (X = I/Br/Cl, simultaneous Br (2 mol%) and Cl (6 mol%) substitution) perovskite channel layers. (ii) Illustration of the passivation effects of a V_I defect by a Cl anion.[63] Reproduced from ref. 63 with permission from the Springer Nature. (f) Schematic of the optimized FPEA-modified $FASnI_3$ FET structure. The insets show the structure of $FASnI_3$ and the chemical structure of PEAI and F-PEAI.[67] Reproduced from ref. 67 with permission from the American Chemical Society. (g) Transfer characteristics at low temperature (80 K) of the devices with Au, PEDOT: PSS, and PFBT-modified Au as source/drain electrodes (inset: FET device configuration).[77] Reproduced from ref. 77 with permission from the Wiley-VCH GmbH.

10^8 (Fig. 3a-ii), which has been compelling.[37] The SnF_2 additive in the precursor solution alleviates the p-type self-doping effect induced by the oxidation of Sn^{2+} to Sn^{4+}, and produces high-quality and uniform films by regulating the crystallization rate. Furthermore, the team selected a stronger hole inhibitor antimony fluoride (SbF_3) to replace tin fluoride (SnF_2) in trace amounts, which can alleviate the phase segregation and deep defects caused by excessive SnF_2, and the prepared film has better crystallinity.[38] Huo *et al.* reported a van der Waals epitaxial borderless ultra-thin $CsPbBr_3$ single crystal FET in which sample transfer is assisted with PVA polymer, showing μ_{hole} and I_{on}/I_{off} of 0.32 cm^{-2} V^{-1} s^{-1} and 6.7 $\times$ 10^3, respectively. In addition, at low temperatures, the μ_{hole} and I_{on}/I_{off} can be increased to 1.04 cm^{-2} V^{-1} s^{-1} and 1.3 $\times$ 10^4, respectively.[39] Among them, vdW epitaxy is not strictly limited to the lattice matching between the epitaxy layer and the substrate, which is conducive to the growth of large-area 2D single crystals with excellent quality. Furthermore, $CsPbBr_3$ single crystals selectively nucleate on the surface of the electrode material silver, resulting in a perovskite/silver heterostructure, which will provide a well-contacted semiconductor/metal interface. The Ag particles, with a small curvature radius and high surface energy on the surface of SiO_2, can induce $CsPbBr_3$ to nucleate and grow into large single crystals, then the single crystal connect Ag particles to form BGBC devices with mobility up to 2.3 cm^{-2} V^{-1} s^{-1}.[40] With the help of gas phase epitaxial deposition technology, $CsPbBr_3$ can grow a macroscopically large-area and thick-controlled single crystal film with a smooth and flat surface and almost no defects (Fig. 3b-i). In the prepared coplanar geometry device (Fig. 3b-ii), the long channel is not only beneficial to the investigation of the inherent transmission characteristics, but also helps to reduce the influence of contact resistance. The intrinsic mobility is 30 cm^{-2} V^{-1} s^{-1} at room temperature, and increased to 250 cm^{-2} V^{-1} s^{-1} when the temperature is declined to 50 K.[41] However, the potential challenge of all inorganic 3D-perovskite devices stems from the inherent phase instability. For instance, $CsSnI_3$ is essentially a phase change material with four polymorph states: yellow phase (Y) with a one-dimensional double chain structure and black orthorhombic phase (B-γ) with a three-dimensional perovskite at room temperature; at 425 K, the Y phase is transformed into black cubic phase (B-α); and the black phases (B-α, B-β, B-γ) can transform reversibly through melting and crystallizing.[36] The B-γ crystal is easily affected in ambient condition, can be quickly converted into a polycrystalline Y phase, losing the monocrystalline properties, and eventually decompose.[36,42] A FET based on conjugated polymer PFO and $CsPbI_3$ nanocrystals composite films exhibit typical *I–V* characteristics at temperatures 200–300 K, but the saturation characteristic is lost at temperatures below 200 K, which may be attributed to reduced conductivity of the PFO polymer and the phase transition of $CsPbI_3$ (from a cubic phase at $T > 300$ K to a tetragonal phase with a temperature between 150 K and 300 K, to an orthorhombic phase at $T < 150$ K).[43] The phase transition weighs heavily on the performance and even limits the application of the materials, such as degrading the switching operation in real-time.[44] The preparation of low-dimensional perovskites with surface effects and nano-effects, such as quantum dots, nanosheets, nanorods, and nanowires, can improve phase stability.[45] Adding phase stabilizers or passivators is also an effective strategy. For instance, Lee *et al.* synthesized a stable cubic phase by doping the bismuth iodide as the phase stabilizer in $CsPbI_3$ and added KBr as the passivating agent to decrease the defect density, showing high hole mobility ($\approx$10 cm^{-2} V^{-1} s^{-1}) and on/off current ratio (10^3).[44]

Compared with inorganic three-dimensional perovskites, organic–inorganic hybrid 3D perovskites are rarely used in the field of FETs, it is dwarfed by its booming development in other fields (*i.e.*, solar cells, light emitting diodes, and photoelectric detectors), the reason behind this may be the gate field effect shielding caused by ion migration.[46] Such ion migration resulting in an unusual behavior, including current–voltage hysteresis, large dielectric responses at low frequencies, and reduced effective carrier mobility, while ions accumulating at the interface between electrode and semiconductor under a long-time bias will cause the healing of vacancies and reduce contact resistance so as to rise the current.[47–49] Numerous studies have been conducted on methylammonium lead iodide ($CH_3NH_3PbI_3$), as it shows a very outstanding power conversion efficiency in solar cell applications, and its crystal structure is displayed in Fig. 3c-i. The inorganic components of the crystal are corner-sharing $[PbI_6]^{4-}$ octahedron units, with $CH_3NH_3^+$ cations inserted into the octahedral space as A-site cations, accompanied by 12 iodide ions. At room temperature, the $CH_3NH_3PbI_3$ lattice is in equilibrium concentration of anionic (V_I^-) and cationic (V_{Pb}^{2+} and V_{MA}^+) vacancies and supports vacancy-mediated diffusion. There are three main ion transport behaviors (Fig. 3c-ii): the migration of the I^- along the edge of the $[PbI_6]^{4-}$; the Pb^{2+} migrates diagonally along the $\langle 110 \rangle$ direction in the cubic cell units; the MA^+ migrates to the vacancies of the nearby A-site cations.[47,50] The polarization effect is sensitive to ion migration. As shown in Fig. 3d, when the gate voltage is applied to provide energy, the dipolar molecule cations are arranged by moving ions, thus generating electric field shielding, inhibiting the accumulation of carriers, and obstructing the channel conduction.[51] The ions mainly migrate along the grain boundaries of the polycrystalline perovskites (grain boundary polarization), and further, the relatively conductive grains are isolated by the electrically insulated grain boundaries, causing enhanced space charge polarization along the grain boundaries.[51,52] When the temperature changes, the crystal structure of the $CH_3NH_3PbI_3$ changes from the orthorhombic phase to the tetragonal phase, which has a larger cage scale and is conducive to the movement of I^- or MA^+.[53] These ions cause electron disturbances, trapping electrons or dispersing their motion. It has been found that doping small cations such as Cs^+ can alleviate lattice strain, which roots in the size mismatch between A-site cations and lead halide cages in perovskites, and strain relaxation occurs through ion vacancy, thus inhibiting ion migration.[48] The ferroelectric copolymer poly(vinylidene fluoride-*co*-trifluoroethylene) (PVDF-TrFE) is used as the dielectric, which

is expected to overcome the problem of gate field shielding caused by ion migration. The dipole polarization in the ferroelectric dielectric layer forms a local electric field while the gate is positively biased, which can induce a higher surface charge density (7–8 μC cm^{-2}) than $MAPbI_3$ (5 μC cm^{-2}), so even if the gate field shielding effect still exists, it can accumulate charge at the interface and form a conductive channel.[54,55] Moreover, the FETs operating with DC bias at all three electrodes induces strong ion migration and MA^+ cation polarization, but AC bias at the gate, especially at high frequencies, is supposed to hinder the ion migration and polarization of MA^+, thereby improving device efficiency.[49] Interestingly, the hysteresis in the current–voltage loop caused by ion migration in perovskites is detrimental to the performance of FETs but can confer artificial synaptic memory states on different time scales.[56,57] The ion migration can be characterized by changing the voltage sweep rate, because the ions and charge carriers flow simultaneously at a slow sweep rate, while at a fast sweep rate, only the drift of charge carriers happens.[58]

Despite the limitation of ion migration, the enthusiasm for researching 3D halide perovskites based on methylamine spacer cations has not diminished. Early studies have found that the $MAPbI_3$ TFT device has bipolar charge transfer behaviors, and mainly exhibits p-type behaviors, which enable it to absorb light energy and produce electron–hole pairs upon light irradiation.[59] This interesting phenomenon makes $MAPbI_3$ play an important role in photovoltaic systems. Yu *et al.* developed a vertical $MAPbI_3$/ITO Schottky junction transistor with the injection-controlled gating mechanism that is more easily transported to the top drain after electron injection, avoids the influence of ion migration at the interface of semiconductor/dielectric layer, and the vertical channel facilitates the formation of a strong electric field at low voltage.[60] Under the same conditions, mixed-halide perovskite films often show better mobility than their single-halide perovskite counterparts. On the one hand, partial chlorine substitution may play a major role in the improvement of performance, because chlorine acts as a crystallization-retarding and -directing agent to regulate the crystallization process of perovskites, and the high quality of the film is usually shown with a uniform morphology.[61,62] The Br anion competes with the I anion and forms stronger coordination with metal ions, regulating the nucleation and crystallization kinetics of perovskite films.[63] On the other hand, the mixed-halide perovskites tend to form polycrystals, producing low carrier scattering, and have a long carrier diffusion length of about 1 μm.[64] Zhu *et al.* reported a tin-based mixed halide 3D perovskite ($MASnX_3$, X = I, Br, Cl) (Fig. 3e-ii), in which the use of tin-based perovskites can significantly reduce Fröhlich interactions due to the polarity of the lead-halide bond, thereby increasing room-temperature charge-carrier mobility.[63] A small amount of Br and Cl co-replacing can improve film quality and passivate vacancies. Negligible hysteresis can be observed at different scanning rates (from 0.4 to 4 V s^{-1}), with high mobility (20 cm^2 V^{-1} s^{-1}), high on/off current ratio (10^7), and low threshold voltage (0 V) (Fig. 3e-i). The formamidine cation (FA^+) as an A-site cation can be used to prepare 3D perovskites with low band gaps, such as $FAPbI_3$ with a band gap of 1.4 eV and $MAPbI_3$ with a band gap of 1.57 eV, and also with a small injection barrier.[65] Based on the mixed-cationic $FA_{0.5}MA_{0.25}Cs_{0.25}PbI_3$ perovskite FETs, which show lower off current compared to $MAPbI_3$, resulting in a higher on/off current ratio (about an order of magnitude improvement).[66] The multi-cationic strategy also involves the addition of large organic ligands namely, on the basis of the 3D halide perovskites, introducing the organic cationic ligands used for 2D perovskites, and can realize ordered crystallization. High-performance (the μ of 15.1 cm^2 V^{-1} s^{-1} and minimal hysteresis) and stable 3D $FASnI_3$ were reported based on the additive engineering strategy (Fig. 3f), that is, adding the organic ammonium salt additive (PEAI or FPEAI) into the precursor solution to obtain a highly crystalline film with a better orientation, meanwhile adding a small amount of SnF_2 to reduce tin vacancy by inhibiting the oxidation of Sn^{2+}.[67–69] It is also noteworthy that the SnF_2 compensator can improve performance efficiently thanks to the hydrogen bonds between the F^- and the FA^+, and other counterparts such as SnI_2 or $Sn(Ac)_2$ have no hydrogen bonding assistance.[68] The FPEAI-modified devices work much more efficiently than the PEAI because FPEAI can be adsorbed on the surface of $FASnI_3$ to form a stronger Sn–I bond, forming a more hydrophobic surface, and can also passivate the defects at grain boundaries, resulting in a lower trap density.[67,68] Such multi-cationic engineered high-quality films with large organic ligands can not only promote carrier transport, but also reduce the contact barrier with the top electrodes.[69] Also, the band bending of Sn–Pb mixed perovskites result in a reduced band gap because the ionic radius of Sn^{2+} (1.35 Å) is smaller than that of Pb^{2+} (1.49 Å).[70] One example has mixed A-site cations (Cs–FA) and mixed B-site metals (Pb–Sn), with the optimal combination being $Cs_{0.15}FA_{0.85}Pb_{0.5}Sn_{0.5}I_3$, and exhibits a high hole mobility of 5.4 cm^2 V^{-1} s^{-1} at room temperature.[71] The mechanism for the inhibition of ion migration has been clarified: (1) when 25% Sn replaces Pb, there is a transition from n-type transport to p-type transport, and the negative gate bias leads to the accumulation of positively charged ions (A^+ and B^{2+}), and the mobility rate of positively charged ions is lower than that of halogen-based ions in Pb-based perovskites; (2) the optimized CsFA component mitigated MA^+-induced dipolar disorder.[71,72]

The monocrystalline films of hybrid perovskites have better performance than polycrystalline ones in terms of carrier mobility, diffusion length, and defect inhibition. The polycrystalline thin films obtained by spin coating are not compatible with the traditional lithography process, and subsequent patterning and integrated device arrays are limited. Some studies have indicated that films prepared by physical vapor deposition usually have better quality than those prepared by solution methods, and the thickness can be precisely regulated.[73] For example, $MAPbI_3$ perovskite films prepared with the aid of low-temperature vapor deposition manifest high surface coverage, low roughness, and large grain size.[74] The film deposited at a slow rate yields a low nucleation density with large grain sizes, while the film deposited at a fast rate shows a high nucleation density.[33] Wang *et al.* deposited PbI_2 and MAI step by step and

selectively controlled crystal nucleation and growth by using alternate hydrophilic/hydrophobic patterns on the substrate surface to obtain a regular array of perovskite microcrystals.[75] The FET transfer characteristics are n-type (high negative gate bias allows a slight p-type), and the on/off current ratio is on the order of 10^6. Using the space-constrained inverse temperature crystallization method to produce morphologically super-smooth top and bottom planes, results in a high-quality semiconductor/dielectric interface in the channel.[76] Field-effect mobilities at room temperature are as high as 4.7 and 1.5 $cm^2\ V^{-1}\ s^{-1}$ in p- and n-channel devices, on/off current ratios are 10^4 and 10^5, respectively, and have low on–off voltages. $MAPbBr_3$ seems to be more prone to ion migration than $MAPbI_3$ under similar process conditions, so relatively little research has been done on $MAPbBr_3$. High-quality $MAPbBr_3$ single crystal is grown with an optimized antisolvent gas-assisted crystallization method, and the conductive polymer poly(3,4-ethylenedioxythiophene)–poly(styrenesulfonate) (PEDOT:PSS) and the self-assembled single layer pentafluorophenthiophenol (PFBT) was used as the surface modification layer to eliminate the adverse electrochemical reaction between the semiconductor and the gold electrode.[77] It can be observed that the on-current increases significantly, the off-current decreases, the on/off current ratio increases from 10^2 to 10^6 over that of the device with unmodified Au electrodes, and the hole mobility extracted by the transconductance method can reach $\approx$15 $cm^2\ V^{-1}\ s^{-1}$ at a saturation state (Fig. 3g). The vertical field-effect transistors (VFETs) based on a graphene/$MAPbBr_3$ single crystal Schottky junction were prepared by Left *et al.*, which can not only shorten the channel length to extract a high carrier mobility (23.4 $cm^2\ V^{-1}\ s^{-1}$), but also change the height of the Schottky barrier at the Schottky junction interface by modulating the gate voltage, promoting or preventing hole injection, and making the device perform bipolar transmission.[78]

The phenomenon that most 3D perovskite transistors exhibit field-effect behaviors and superior performance at low temperatures is related to the elimination of the shielding effect. It is still a limiting factor for the development of 3D perovskites, and the optimal solution has not yet been found. The investigations of temperature-dependent effects explain charge transfer mechanisms in the perovskite materials, which helps to better understand the relationship between mobilities and temperature. Soci and his co-workers' research found that the transfer performance of $MAPbI_3$ is strongly temperature-dependent.[46] There is almost no gate modulation behavior when the temperature is above 198 K, the n-type transmission is displayed at temperatures below 198 K, the p-type transfer is observed at 98 K, and a bipolar transmission behavior is displayed at 78 K (Fig. 4a-i). The mobilities corresponding to different temperatures are shown in Fig. 4a-ii. It can be observed that the hole and electron mobilities increase nearly 100 times when the temperatures are lower than 198 K, which is related to the elimination of the shielding effect induced by ion migration. The MA^+ cation-related phonon interaction is quenched at low temperatures. The discrepancy in mobilities is also related to the phase structures at different temperatures (Fig. 4a-iii), the calculated result shows that the mobility of the orthorhombic phases is better than that of the tetragonal phases. The work of Senanayak *et al.* suggests that the mobilities in different temperature regions meet distinct power-law behaviors ($\mu_{FET} \sim \mu_0 T^{-\gamma}$), which are closely related to the film quality.[79] Specifically, the smaller particle sizes lead to a larger film mobility exponent and a higher defect concentration (Fig. 4b-i). In the dielectric mismatch spectra (Fig. 4b-ii), the characteristic relaxation frequency appears at $T > 240$ K, indicating that the charge transport is affected by ion migration. The inhibition of ion migration in region II is attributed to the reduction of MA^+ polarization disorder, while the orthorhombic phase is dominant in region I. It is important to note that mobilities do not always increase with decreasing temperature. Fig. 4c and d-i both show the unconventional mobility-temperature dependence. In Fig. 4c, the mobility increases with the decreasing temperature, showing a power exponential relationship of $\mu \sim T^{-2.35}$ in the range of 260 K to 300 K.[33] The abnormal phenomenon below 260 K comes from the thermal activation of the current in the phototransistors exposed to the 473 nm laser. Fig. 4d-i shows that the expected mobility-temperature dependence did not occur in region 2, which can be explained as follows: (1) the prepared perovskite is a single crystal with low defect density and is barely influenced by defects at a low temperature. (2) With the decrease in temperatures, ion migration is weakened, and ions gather at the semiconductor/dielectric interface under the electric field. These mismatched ions can create scattering as charge impurities, resulting in the reduction of mobilities in region 2. The increased mobilities of region 1 are mainly due to the limited hindrance of phonons and ions to carrier transport at very low temperatures (Fig. 4d-ii).[39] Usually, the temperature exerts a great impact on the performance of 3D halide perovskite transistors, which is not conducive to long-term development.

4. Two-dimensional halide perovskite FETs

To date, although lots of halide perovskite FETs with promising performance are 3D structures, the pioneering halide perovskite FETs are using layered hybrid structures, $(C_6H_5C_2H_4NH_3)_2SnI_4$ (Fig. 5a). Back in 1999, Mitzi combined the advantages of easy self-assembly of PEA and high carrier mobility of inorganic semiconductors, and since then has stimulated the research enthusiasms of 2D hybrid halide perovskites. According to whether the organic cations are monoammonium, divalent, or alternating cation, the Ruddlesden–Popper (RP) phases ($A'_2A_{n-1}B_nX_{3n+1}$), the Dion–Jacobson (DJ) phases ($A''A_{n-1}B_nX_{3n+1}$), and alternating cations in the interlayer (ACI) phase ($A'A_nB_nX_{3n+1}$) are formed respectively, and the structure diagram is shown in Fig. 5b.[80,81] Layered PR phase $(PEA)_2SnI_4$ transistors operate in a cumulative mode when a negative gate bias is applied, exhibiting a p-channel transmission behaviour with the mobility of 0.62 $cm^2\ V^{-1}\ s^{-1}$, which comparable to amorphous silicon deposited under vacuum.[82] In the subsequent research, the effects of fluorine substitution at different positions of the benzene ring was investigated based on

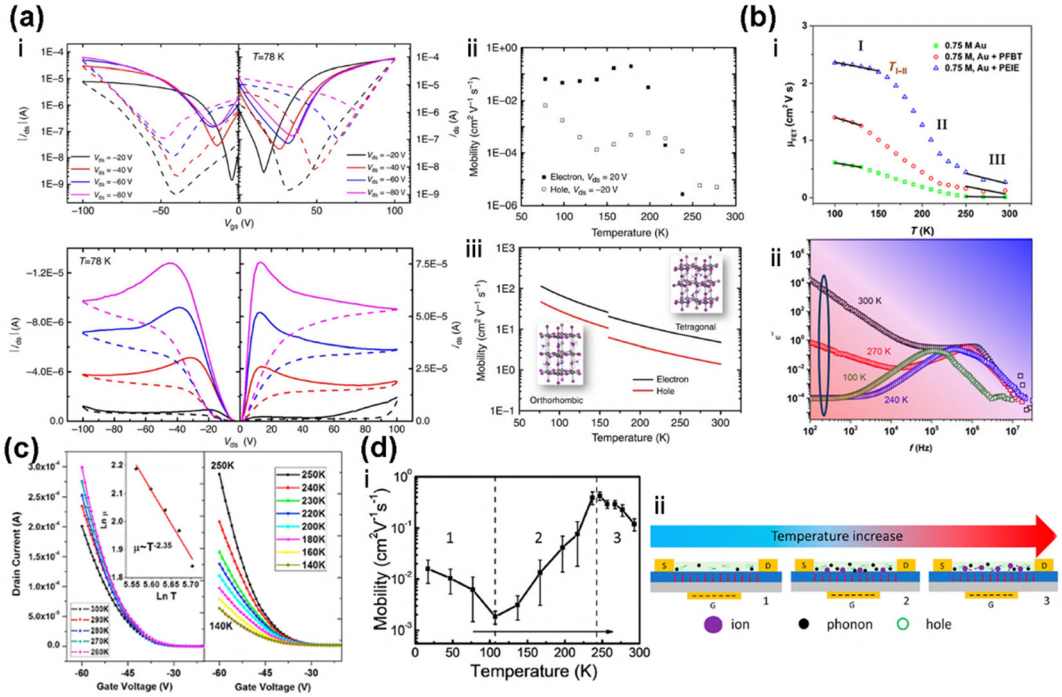

Fig. 4 (a) (i) Ambipolar transfer (top) and output (bottom) characteristics of $CH_3NH_3PbI_3$ FETs obtained at 78 K. Solid and dashed curves are measured with forward and backward sweeping, respectively. (ii) Temperature dependence of field-effect electron and hole mobilities. (iii) Calculated temperature dependence of hole (red curves) and electron (black curves) mobility in tetragonal (T = 300 to 160 K) and orthorhombic (T = 160 to 77 K) phases of $CH_3NH_3PbI_3$. The crystal unit cells of the two phases are shown as insets.[46] (b) (i) The curves of $\mu_{FET} - T$ with different interlayers at the S–D contacts depicting three different regimes of charge transport with a power law behavior: $\mu \sim \mu_0 T^{-\gamma}$. Region I: inorganic cage vibrational disorder ($\gamma \sim 0.2$ to 0.4); region II: dominated by the polarization fluctuation of MA^+; region III: dominated by ion migration ($\gamma \sim 4.1$ to 5.3). (ii) Corresponding dielectric loss measurement as a function of frequency and temperature.[79] (c) Temperature-dependent transfer curves of $MAPbI_3$/C8BTBT hybrid FETs in the dark, the inset shows a band-like behavior in the relationship between mobility and temperature above 260 K.[33] (d) (i) Temperature dependence of the transistor mobility. (ii) Schematic diagram of the operating mechanism regarding the charge carrier transport.[39] Figures reproduced with permission from: (a) ref. 46. Copyright 2015, Springer Nature; (b) ref. 79. Copyright 2017; (c) ref. 33. Copyright 2016, Elsevier; (d) ref. 39. Copyright 2017, American Chemical Society.

$(PEA)_2SnI_4$.[83] On the one hand, the crystal structures can be modified, that is, the average length of the Sn–I bonds can be changed to reduce octahedral distortion as much as possible, and the structures of $(4\text{-FPEA})_2SnI_4$ and $(PEA)_2SnI_4$ are most similar. On the other hand, the fluorine substitution can improve the solubility and the underlying hybrid structures, thus affecting the film quality. The grain sizes of $(3\text{-FPEA})_2SnI_4$ and $(4\text{-FPEA})_2SnI_4$ are relatively large, and the FET performances are better. Apart from regulating the crystal structures, plentiful efforts have been made in the fabrication methods. Although the solution methods have advantages in terms of operation and cost, the quality and reproducibility of the films are affected by solubility and wettability, which indirectly affect the device performance. After $(PEA)_2SnI_4$ was vacuum vapor hot deposited on the silicon wafer treated with UV-O_3 and octadecyltrichlorosilane (OTS), the film morphology and crystallinity can be improved, and the electrical performances of the FET also are improved (mobility of 0.78 $cm^2\ V^{-1}\ s^{-1}$, threshold voltage of −1.7 V, and on/off current ratio of 4.2×10^5).[84] As another promising fabrication method, the low-temperature melting process is also relatively simple and economical, as well as it does not involve problems of solubility and solvent removal.[85] The mobilities ($\mu_{sat} = 2.6/\mu_{lin} = 1.7\ cm^2\ V^{-1}\ s^{-1}$), on/off current ratio (10^6), and reproducibility of $(3/4\text{-MeOPEA})_2SnI_4$ FETs obtained by low-temperature melting are improved.[85]

$(PEA)_2SnI_4$, as the most widely explored 2D tin-based hybrid perovskite candidate, is also looking for breakthroughs, especially in addressing low mobilities caused by carrier defects, poor film quality, contact resistance, and injection barriers. Most FET devices based on $(PEA)_2SnI_4$ are mainly fabricated using solution-processing techniques. Therefore, understanding the precursor's colloidal chemistry and crystallization kinetics is critical. Ryu *et al.* introduced MACl into the $(PEA)_2SnI_4$ precursor solution, which facilitated the formation of $(PEA)_2SnI_4$–MACl intermediate complexes. This approach not only mitigated the issues of undesired rapid crystallization but also enabled the large intermediate molecules to serve as nucleation sites, thereby promoting the Ostwald ripening process and the growth of larger crystalline.[86] Moreover, precursor aging—a pre-treatment step for precursor solutions—has been demonstrated to be essential. Opportune aging facilitates the conversion of unreacted and aggregated large clusters in the fresh precursor into smaller, more stable colloids, thereby eliminating the poor coordination of SnI_2 as well as improving

both nucleation and crystal growth.[87] Interestingly, high performance FET devices have also been obtained by improving the quality of the semiconductor–dielectric interface. The introduction of a self-assembled monolayer rich in ammonium iodide (NH_3I-SAM) between the silica dielectric and the $(PEA)_2SnI_4$ semiconductor induces the inorganic layer to align parallel to the substrate, which facilitates more orderly crystallization and enhances carrier transport (Fig. 5c). Moreover, the composition of the NH_3I-SAM eliminates excess Sn^{2+} that causes hysteresis, reducing the chance of carrier scattering and increasing the hole mobility to 5.7 $cm^2\ V^{-1}\ s^{-1}$. Furthermore, the hole injection barrier was reduced by inserting molybdenum oxide (MoO_x), and the polymer Cytop was replaced as the gate dielectric layer to optimize the FET devices with the TCTG structure. The optimized mobility is as high as 15 $cm^2\ V^{-1}\ s^{-1}$.[88] In a follow-up study, the $(PEA)_2SnI_4$ film was prepared by the combination of vacuum vapor deposition technology and hydrophobic octadecyl trichlorosilane self-assembled monolayer (OTS-SAM) surface treatment, while the solution method has limitations in hydrophobic surfaces.[12] The contact resistance between the semiconductor layer and the source/drain electrodes will hinder the judgment of the true electrical performance of the transistors. Long-channel perovskite field-effect transistors (channel length L = 1–3 mm) help minimize the adverse effects of contact resistance and electrical polarization (*i.e.*, ion drift or displacement in the perovskite lattice caused by an external electric field).[41] To evaluate the true carrier mobility of $(PEA)_2SnI_4$ FETs, Matsushima *et al.* designed a device with a long channel.[14] The results showed that both mobility of the p-channel and n-channel increased with the increase of L, and remained constant in the larger L region, from which the extracted hole and electron mobility are 26 and 4.8 $cm^2\ V^{-1}\ s^{-1}$, respectively. This is because the lengthening of the L reduces the contribution of the contact

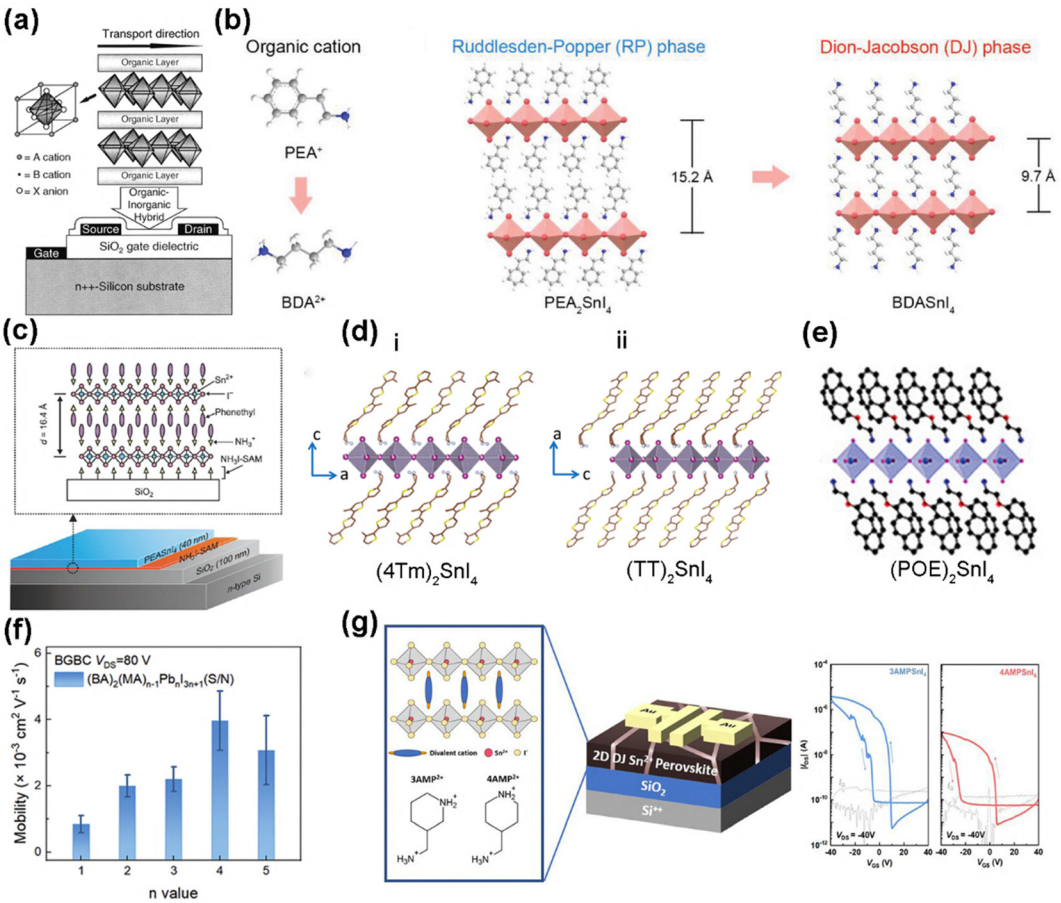

Fig. 5 (a) Schematic diagram of the first solution-treated two-dimensional layered halide perovskite FET structure.[82] (b) Schematic illustration of the lattice structure of $BDASnI_4$ (DJ phase) and $(PEA)_2SnI_4$ (RP phase) perovskites.[80] (c) Schematic of the $(PEA)_2SnI_4$ perovskite film grown on NH_3I-SAM.[88] (d) 2D RP phase halide perovskites featured with conjugated ligands. The side view of the $(4Tm)_2SnI_4$ crystal structure for (i) and the $(TT)_2SnI_4$ crystal structure for (ii).[92] (e) 2D perovskite based on a fused ring π-conjugated pyrene-*O*-ethyl-ammonium (POE) ligand.[93] (f) The statistical data of $(BA)_2(MA)_{n-1}Pb_nI_{3n+1}$(S/N) TFTs for mobility. The error bars represent the SD from five individual devices.[96] (g) The crystal structure of DJ phase perovskite ($3AMPSnI_4$ and $4AMPSnI_4$) and chemical structure of corresponding ligands (left), the schematic of BGTC FET based on DJ phase perovskite (middle), and the transfer characteristic curves of $3AMPSnI_4$ and $4AMPSnI_4$ FETs (right).[101] Figures reproduced with permission from: (a) ref. 82; (b) ref. 80. Copyright 2023, Wiley-VCH GmbH; (c) ref. 88. Copyright 2016, Wiley-VCH GmbH; (d) ref. 92. Copyright 2021, American Chemical Society; (e) ref. 93. Copyright 2023, Wiley-VCH GmbH; (f) ref. 96; (g) ref. 101. Copyright 2024, American Chemical Society.

resistance to the overall resistance. The p-channel and n-channel are gained *via* transforming metal electrodes with different work functions so that they are favorable for hole or electron injection. The mobility-temperature dependence was tested in the temperature range of 20 to −70 °C, and the results indicated that the mobility declined with the decrease in temperatures, which may correspond to a heat-activated mechanism. In most cases, the mobility-temperature dependence is inversely proportional. The layered structures of 2D perovskites inhibit ion migration to a large extent, so the reason for the increase of carrier transport capacity at lower temperatures may be that the crystal structure is frozen, so the lattice vibration is slowed down, and the lattice distortion is reduced correspondingly.[89] Hu *et al.* found that the carrier transport mechanism is different in the high-temperature region (280–300 K) and the low-temperature region (70–260 K).[90] The activation energy of the high-temperature region is one order of magnitude higher than that of the low-temperature region. The low activation energy at low temperatures sheds light on shallow defects dominating. With the increase in temperatures, most shallow traps are filled with activated carriers, but the hysteresis is more obvious, indicating that deep traps dominate in the high-temperature regions.

Recently, π-conjugated organic ligands inspired by phenylethylamine have attracted extensive attention. Bulky π-conjugated organic semiconductor ligands with a relatively larger dielectric constant in 2D perovskite can alleviate dielectric mismatch between the organic ligand layer and the adjacent inorganic octahedral frame, and can be inserted into the lattice of halide perovskites to modify the crystal structure and act as natural protective layers to improve stability. Gao *et al.* pioneered a 2D tin-based perovskite $(4Tm)_2SnI_4$ based on linear π-conjugated oligothiophene ligands, the FET characteristic showed an improved mobility of 2.3 $cm^2\ V^{-1}\ s^{-1}$ compared to pure $(PEA)_2SnI_4$ without any treatment assistance.[91] The side view of the $(4Tm)_2SnI_4$ crystal structure is displayed in Fig. 5d-i. There are two main reasons for the increase in performance. One reason is the presence of electrostatic interactions and hydrogen bonding between amino group and iodine, which leads to a shorter Sn–I bond length in $(4Tm)_2SnI_4$ (3.11 Å) than that in $(PEA)_2SnI_4$ (3.13 Å), as well as reduced N–I distance. Another reason is that the larger grain size reduces the number of grain boundaries, thereby decreasing defect density and suppressing ion migration. Further, for the molecular design of conjugated ligands, TT was synthesized using fused-thiophene rings with larger conjugated planes (Fig. 5d-ii). The introduction of TT molecular reduces the nucleation density, successfully regulates the crystallization kinetics of perovskite, and obtains the $(TT)_2SnI_4$ perovskite films with orderly crystallization and large grain size, the FET mobility up to 9.35 $cm^2\ V^{-1}\ s^{-1}$ and the on/off current ratio is more than 10^5.[92] In addition, by analyzing the crystal structure, it is found that $(TT)_2SnI_4$ has a larger bond length distortion index and a smaller Sn–I–Sn angle than $(4Tm)_2SnI_4$, and the in-plane lattice is more contracted so that the structure is more stable. Extension of the ligand conjugated planes and corresponding enhanced intermolecular interactions help adjust nucleation dynamics. Zhang *et al.* synthesized 2D perovskite based on a fused ring π-conjugated pyrene-*O*-ethyl-ammonium (POE) ligand (Fig. 5e) with large conjugated planes, and employed a high-boiling-point Lewis alkaline solvent to control crystallization.[93] Larger grains have been obtained, and the resulting FET device showed excellent stability and repeatability.

2D lead-based perovskites have been less studied than 2D tin-based perovskites, which may be related to the stronger Fröhlich interactions, but it is equally important for the development of perovskite transistors.[94] Tin and lead are located in the same main group, have similar outer electronic structures and ionic radii, and mixing in any proportion causes little lattice distortion. Sn–Pb mixed perovskite $(PEA)_2Sn_xPb_{1-x}I_4$ can significantly improve film quality and environmental stability.[95] Because the Lewis acidity of Sn^{2+} is stronger than that of Pb^{2+}, the rapid crystallization of tin-based perovskite leads to poor film quality, while the Sn–Pb mixed perovskite is conducive to improving the crystallinity. The improvement of environmental stability is reflected in which the Pb–I bond is stronger than the Sn–I bond, and the $[PbI_6]^{4-}$ octahedra do not provide I^- for further oxidation of SnI_2 when the perovskite degrades to generate SnI_4. Qiu *et al.* prepared 2D lead-based halide perovskites $(BA)_2(MA)_{n-1}Pb_nI_{3n+1}$ with different n values and used NH_4Cl as an additive to induce ordered crystallization, and SnO_2 as a spacer layer to improve charge injection.[96] The mobility raised with the increase of the n value and shows that the champion mobility ($5.73 \times 10^{-3}\ cm^2\ V^{-1}\ s^{-1}$) at room temperature when $n = 4$, the on/off current ratio was 10^4, and the hysteresis was negligible (Fig. 5f). With the increase in the number of repeats (n value), the optical band gap and exciton binding energy decrease, which is expected to further increase the mobility of organic–inorganic hybrid perovskite transistors.[82,97] The 2D perovskites (n = 1) tend to be parallel to the substrate, which is conducive to lateral charge transport, and quantum wells formed by alternating organic/inorganic layers can effectively prevent vertical ion migration. However, the vertical transport of charge is also limited due to the existence of quantum well structures. Appropriately increasing the n value to form a quasi-2D perovskite could promote vertical charge transport and further improve mobility. By mixing NMA^+ (1-naphthylmethylamine cation) and FA^+ to separate single, double, and multilayer inorganic octahedral planes $[PbI_6]^{4-}$, self-organizing multi-quantum well perovskite $NMAFAPb_2I_7$ ($NFPI_7$) is designed to endow perovskite transistors with bifunctional characteristics, not only presenting high mobility ($>20\ cm^2\ V^{-1}\ s^{-1}$) and on/off current ratio ($>10^6$), but also showing efficient and stable infrared or near-infrared emission.[98] Guo *et al.* compared some basic properties of 2D $(PEA)_2PbI_4$, quasi-2D $(PEA)_2(MA)_{n-1}Pb_nI_{3n+1}$ (n = 6), and 3D $MAPbI_3$.[13] Among them, the reduction of dimension leads to smoother film, prolonged carrier lifetimes, and enhanced environmental stability; however, vertical conductivity increases as the dimensionality rises. It can be seen that quasi-2D perovskites are conducive to vertical charge transport while maintaining the advantages of low-dimensional perovskites.

The diamine cation in 2D DJ phase perovskite is directly connected to the upper and lower inorganic layers, which not only eliminates the van der Waals gap in the RP phase and

weakens the quantum well effect, but also enhances the electron coupling between the layers by shortening the distance of the inorganic layers, which is conducive to the out-of-plane charge transfer. Nevertheless, little attention is given to the DJ phase perovskites. Recently, the DJ phase perovskite $BDASnI_4$ prepared with 1,4-butanediamine (BDA) as an organic ligand showed a much lower average out-of-plane effective mass ($0.159m_0$) than $(PEA)_2SnI_4$, indicating that electron transport in the out-of-plane direction of $BDASnI_4$ is more favourable. The exciton binding energy of $BDASnI_4$ (56 meV) is also much smaller than that of $(PEA)_2SnI_4$ (174 meV), which is attributed to the weakening of the quantum well effect.[99] Low exciton binding energy may not be conducive to the fabrication of light-emitting devices, but efficient exciton separation and charge transport are suitable for FETs. The bandgap–temperature relationship model showcased that the band gap of $BDASnI_4$ is dominated by thermal expansion when the temperature is lower than 140 K (thermal expansion affects the band structure by changing the lattice constant), and dominated by the electron-longitudinal optical (LO)–phonon interaction (the electron–phonon interaction affects the band structure by lattice vibration) as the temperature increases.[94,99] $(PEA)_2SnI_4$ is dominated by thermal expansion below 120 K, and as temperature rises is influenced by both thermal expansion and the electron–phonon interaction. Meanwhile, the energy difference ($\Delta_{EP} = E_{EP320K} - E_{EP80K}$) between the bandgaps at 320 K and 80 K of $BDASnI_4$ (−20.07 meV) and $(PEA)_2SnI_4$ (−64.83 meV) are calculated respectively, reflecting the contribution of the electron–phonon interaction for the temperature evolution of bandgap over a temperature range in the perovskite films. The results showed that the contribution of the interaction to BDA is small, indicating that the DJ phase perovskite has a more stable structure and weakens the heat-induced electron–phonon coupling. The advantages of the DJ phase perovskites applied to FET are analyzed from multiple perspectives, and its development is considered to be very promising. Qiu *et al.* proposed a strategy of coordinating alkyl ammonium salt spacers with the NH_4SCN additive to regulate the crystallization process of $BDASnI_4$ films, in which the introduction of a spacer layer helps to reduce defect density.[80] The optimized film has excellent morphology, high mobility (1.61 $cm^2\ V^{-1}\ s^{-1}$), and on/off current ratio (4.7×10^6), and the conduction current of the unpackaged FET is almost unchanged after 150 days in the nitrogen atmosphere. Some studies have investigated the odd–even effects of linear alkyl-chains spacers on charge transport. A very recent result indicates that ligands containing even-numbered alkyl chains (4, 6, or 8) facilitate the formation of layered 2D DJ phase perovskites and exhibit excellent electrical properties. In contrast, ligands with odd-numbered alkyl chains (3, 5, or 7) disrupt the formation of the 2D structure.[100] Compared with aliphatic diamine cations, aromatic diamine cations have a larger dielectric constant, which can effectively reduce the dielectric mismatch between the organic layer and the inorganic layer, thus mitigating the dielectric confinement effect. Park *et al.* prepared 3-(aminomethyl) piperidine tin iodine ($3AMPSnI_4$) and 4-(aminomethyl) piperidine tin iodine ($4AMPSnI_4$) DJ phase perovskites (Fig. 5g).[101] Among them, the difference in the position of aminomethyl group will form different hydrogen bond environment and affect the holistic perovskite lattice. For example, the 3-site aminomethyl-substituted perovskite has smaller layer spacing and better symmetry, so the perovskite lattice is more robust, and the saturation mobility and the on/off current ratio are better than $4AMPSnI_4$. For all this, the types of diamine cationic ligands used for the preparation of the DJ phase perovskites are still few. The material diversity is to be explored, and better performance of their FET devices is further expected.

In compared to polycrystalline perovskites, 2D single crystal perovskites generally show a perfect layered structure, an adjustable band gap, excellent optical properties, significantly reduce defects, and increase carrier diffusion length, which is also an indispensable part of the preparation and fabrication of perovskite FET devices. Dou *et al.* prepared 2D Pb-based atomically thin single crystals $(C_4H_9NH_3)_2PbBr_4$ by a solution method, which exhibited strong light luminescence at room temperature, enriching the 2D hybrid perovskite system.[102] To fabricate transistors on a single crystal $(C_4H_9NH_3)_2PbBr_4$, the large-area single-crystalline graphene film is introduced as protective layer as well as source and drain electrodes.[103] When using acetone cleans the substrate covered with single crystals, the single crystal perovskite covered by graphene is not destroyed, and then the graphene protective layer is slightly damaged by etching as the source/drain electrode, and the gap of about 100 nm is retained, the treatment process is shown in Fig. 6a. Shen *et al.* prepared millimeter-sized single crystal perovskite $(PEA)_2CsSn_2I_7$ by incorporating Cs into 2D hybrid perovskite (Fig. 6b).[8] In the FET performance test, the source–drain current increases as the gate voltage decreases, thus exhibiting p-type transmission with hole mobility up to 34 $cm^2\ V^{-1}\ s^{-1}$ at 77 K. However, such a high carrier concentration might make the semiconductor degenerate, leading metallic characteristics, so the transfer characteristic curve cannot be fully switched off. For $(PEA)_2SnI_4$ single crystal FET, crystals were grown from the precursor solution *via* cooling method that was grew at −25 °C for overtnight.[104] The surface was rough due to the coating residue, and the smooth crystal surface was peeled off by tape to ensure adequate contact with the electrode (Fig. 6c-ii). The champion device has mobility of up to 40 $cm^2\ V^{-1}\ s^{-1}$ and no significant hysteresis (Fig. 6c-i and iii). The results of single crystal FETs with lower grain boundary density, smaller structural disorder, and low defects are closer to the intrinsic carrier transport characteristics of perovskite materials. However, compared with the preparation of polycrystalline thin film devices, the single crystal device is more precise and complex, usually showing low yield in fabrication.

5. Stability issues in perovskite FETs

3D perovskites are generally more susceptible to degradation by environmental influences such as humidity, high temperature,

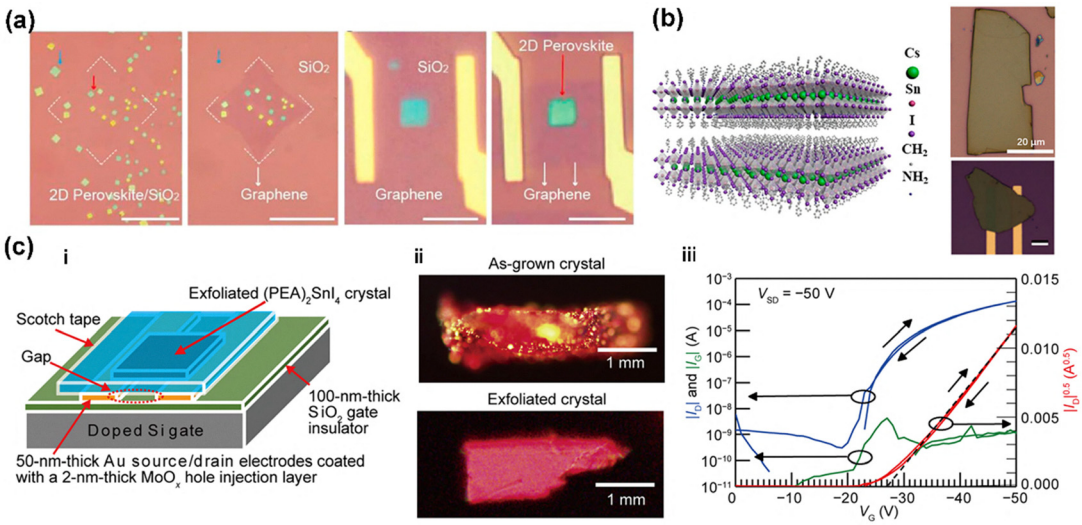

Fig. 6 (a) Optical images of the growth process of 2D $(C_4H_9NH_3)_2PbBr_4$ crystals and the transfer process of a graphene protective layer and 2D $(C_4H_9NH_3)_2PbBr_4$ device with graphene electrodes. The scale bar of the first and the second are 50 μm, and the third and the four are 10 μm.[103] (b) Schematic illustration and optical image of the crystal structure of $(PEA)_2CsSn_2I_7$ perovskite and the optical image of the corresponding device.[8] (c) (i) Schematic architecture of a $(PEA)_2SnI_4$ crystal FET. (ii) Optical microscopy images of the as-grown and exfoliated $(PEA)_2SnI_4$ crystals. (iii) Transfer curves were obtained in nitrogen.[104] Figures reproduced with permission from: (a) ref. 103. Copyright 2016, (b) ref. 8. Copyright 2019, American Chemical Society; (c) ref. 104.

and ultraviolet light.[95] In addition, a screening effect due to ion migration in 3D perovskites field-effect transistors is inevitable. Although the bulky organic ligands in 2D perovskites have been used as natural barriers, challenges remain in terms of long-term stability, environmental operation, and repeatability, which are reflected in the degradation of perovskite layers, ion migration, defects, hysteresis, abnormal device parameters, oxidation, and electrochemical reactions at the interface of semiconductor/electrode, *etc.*

5.1 Vacancy defects

The degradation of perovskite caused by iodide loss is a serious problem, which can generate positively charged iodide vacancies and thus doping semiconductors.[105] For instance, it has been reported that the degradation of perovskite film accelerated when exposed to iodine vapor, long-term thermal annealing, applied large electric field, and affected by superoxide from oxygen and photogenerated electrons. Perovskite degradation leads to positively charged iodine vacancies and free electrons, and resulting in n-type doping. It is a spontaneous process and can accelerated by vacuum and light (Fig. 7a). Encapsulating a thin layer of graphene on the surface of the perovskite layer can prevent the escape of iodide. Zhao *et al.* prepared 2D $(PEA)_2PbI_4$ single crystal perovskite/graphene heterostructures FETs and found that graphene coating can prevent iodide loss to improve the stability of FETs.[105] Due to the difference between the initial Fermi level and the work function, the shift of perovskite single crystals to the graphene channel will cause charge transfer between them. The continuous transfer of excess electrons induces upward bending of the energy band at the interface between the perovskite layer and the graphene, and the Fermi level shifts relative to the Dirac point of the graphene.

An univalent cation (Cu^+) is incorporated into $(PEA)_2SnI_4$ because its ionic radius (77 pm) is smaller than that of Sn^{2+} (118 pm) to avoid causing lattice distortion.[106] The results show that cation segregation along the grain boundary, the grain boundary passivation, and CuI's excellent conductivity are beneficial to hole transport, which improves the transistor performance, with a twofold increase in the mobility and significantly reduced hysteresis. Na^+ also tends to form gaps to passivate grain boundaries and improve film quality.[107] The anion S^{2-} passivates the electron defect caused by iodine vacancy *via* replenishing the V_I, increasing the hole concentration.[10] In addition, xanthate dopants, as the source of S^{2-}, also act as nucleation sites in the films, inducing crystal growth and promoting continuous perovskite films with low surface roughness. The monovalent pseudohalide anion $HCOO^-$ is similar in size to the halide anions and has a higher chelating ability to metal ions. When it partially replaces the I^- in $CsFASnI_3$ perovskite, it can delay the perovskite crystallization process through ion exchange and improve the crystal quality and device performance.[108] Metastable Sn^{4+} can be thermally transformed into Sn^{2+}, and two holes (h^+) are released at the same time. This phenomenon motivated Liu *et al.* to add deliberately SnI_4 as an additive into $(PEA)_2SnI_4$ to form p-doping, and the conductivity is increased by nearly five orders of magnitude.[109] With the increase of doping amount, the grain size also increases gradually. The extra I^- also compensates for the iodine vacancy, so the defect density is reduced. Molecular doping is different from ion doping in that it does not replace any ions in the crystal and can control the charge or defect density without affecting the lattice or band gap.[110] The large ionic radius of formamidine ion often leads to lattice strain, and it has been found that the strain relaxation of the methyl ammonium chloride (MACl) additive on the

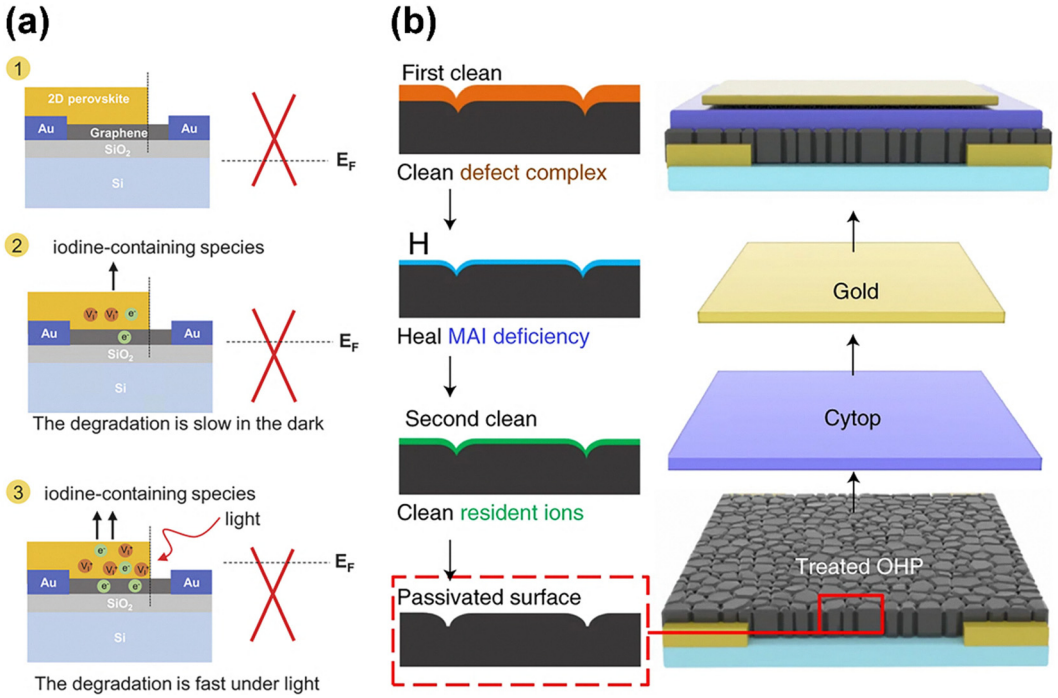

Fig. 7 (a) Schematic showing the mechanism of iodide loss and n-type doping of perovskite and graphene.[105] (b) Schematic of the perovskite FET fabrication process with the cleaning–healing–cleaning (C–H–C) surface treatment of the perovskite layer before deposition of the gate dielectric.[112] Figures reproduced with permission from: (a) ref. 105; (b) ref. 112. Copyright 2020, under exclusive licence to Springer Nature Limite.

perovskite lattice can stabilize the α phase and balance the strain.[111] At the same time, adding tetramethyl ammonium hexafluorophosphate (TMA-PF6) to multidentate anchors uncoordinated lead can not only regulate the morphology and crystallinity of the perovskite film, but also remove the surface defects.

In addition to eliminating the factors that destroy the stability of the FETs from the perovskite structure level, it can also be regulated during the preparation of the films. Sirringhaus and his co-workers invented a surface defect passivation method (C–H–C) by first cleaning the weak adhesion defects on the surface of the $MAPbI_3$ film (C), then healing the halogen vacancy defects formed by the volatilization of the organic halide (H), and finally cleaning again to remove any residual ions introduced by the first cleaning step (C) (Fig. 7b).[112] The combination of polar and non-polar solvents is preferred. The introduction of surface passivation technologies can effectively inhibit ion migration on the surface, and the mobility value is as high as 4 $cm^2\ V^{-1}\ s^{-1}$ at room temperature.

5.2 Degradation mechanism

Matsushima *et al.* monitored the degradation process of the $(PEA)_2SnI_4$ film exposed to oxygen.[113] As time went on, the absorbance decreased, the XRD peak intensity decreased and the peak widened, SEM also showed that the film become discontinuous, but there was no significant change in a dry or a humid nitrogen atmosphere (Fig. 8a). The oxidation-induced degradation process from the precursor to the perovskite to the device is shown in Fig. 8b.[114] Because of the 4f orbital in the Sn atomic structure is not fully occupied, resulting in weak nuclear attraction for the lone pair electrons in the 5s orbital, the existence of active lone pair electrons causes the instability of Sn-based perovskites.[4] Even in a nitrogen-filled glove box, the evaporation of solvents during film deposition may introduce oxygen. When the tin-based perovskite is exposed to water and oxygen, the $[SnI_6]^{4-}$ absorbs water and hydrolyzes into SnI_2, which is easily oxidized to SnO_2 or SnI_4 is formed when there is excess I^-.[95] SnI_4 is first hydrolyzed with H_2O to form HI, which is then oxidized by O_2 to form I_2. When perovskites are exposed to I_2, their degradation accelerates, resulting in the formation of more SnI_4.[115] Degradation root in oxidation leads to lattice instability, which induces the formation of V_{Sn}. Superoxide O^{2-}, generated by the photoreduction of oxygen through photoexcited electrons, can effectively trap electrons and promote the degradation of perovskites.[116] The presence of surface defects leads to poor coordination between halide and metal ions, resulting in the formation of deep defects and ultimately deteriorating device performance.[4] Moreover, the rapid oxidation of Sn(II) by oxygen molecules, which replace halogen defects or gap sites in perovskites, can induce the generation of V_{Sn}, which will cause a P-doping effect and seriously compromise the stability of device operation. Fortunately, the reversibility of P-doping and film recovery for $(PEA)_2SnI_4$ transistors exposed to trace oxygen can be achieved by storing them under vacuum conditions ($\sim 10^{-4}$ Torr) for a period of time.[117]

Polymers are not only excellent candidates for insulation layers, but also commonly used additives for perovskites.

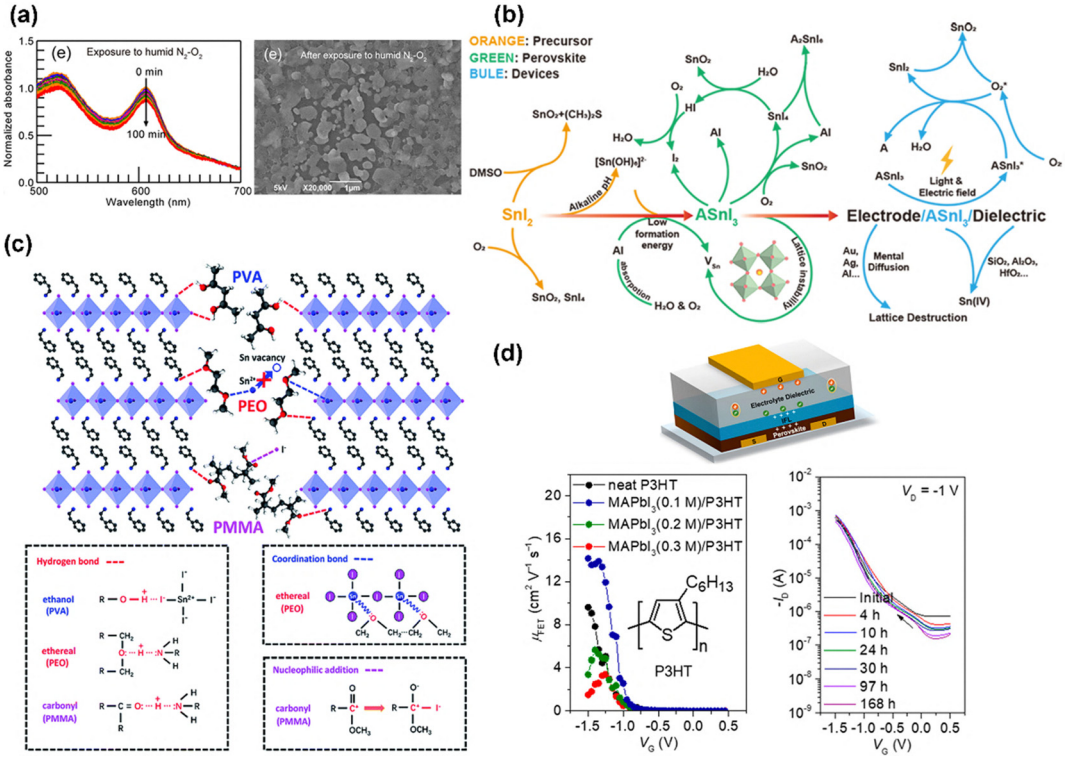

Fig. 8 (a) Evolution of absorption spectra (top) and SEM image (bottom) of $(PEA)_2SnI_4$ films in a humid nitrogen–oxygen mixture.[113] (b) Schematic diagram of the oxidation process during the preparation and operation of Sn-based FETs.[114] (c) Schematic illustrations of the molecular structures of $(PEA)_2SnI_4$, PEO, PVA, and PMMA, which showing polymer-assisted defect passivation effect, and detailed illustrations of the interactions between different functional groups in the aliphatic polymers and $(PEA)_2SnI_4$.[31] (d) Schematic of TGBC transistor devices with working principle, transistor mobility (μ_{FET}) as a function of the gate voltage of the neat P3HT and $MAPbI_3$/P3HT FETs prepared with different concentrations of the $MAPbI_3$ precursor solution (inset is the chemical structure of P3HT), and transfer curves of the $MAPbI_3$ (0.1 M)/P3HT FETs in ambient conditions.[124] Figures reproduced with permission from: (a) ref. 113; (b) ref. 114. Copyright 2023, Wiley-VCH GmbH; (c) ref. 31; (d) ref. 124. Copyright 2023, American Chemical Society.

Multiple interactions between functional groups in the polymer and perovskite components can effectively passivate defects and improve the overall performance of transistors. As shown in Fig. 8c, when blend with the polymers (poly(vinyl alcohol) (PVA), poly(ethylene oxide) (PEO), and PMMA), the hydrogen bonds can be formed between the oxygen-containing groups and the halogen or ammonium ion from perovskites; the coordination bond would happen between the ether bond in PEO and Sn^{2+}; and the nucleophilic addition exists between the ester carbonyl group in PMMA and the halogen in $(PEA)_2SnI_4$. Among them, the Sn–O coordination inhibits the oxidation of Sn^{2+}, thus preventing p-type hole depletion in $(PEA)_2SnI_4$ transistor operation and realizing ambipolar transport.[31,118] Some electronegative small molecules, such as cyanuric acid,[119] chloromethyl phosphonic acid,[120] and pentanoic acid,[121] stabilize the surface Sn^{2+} through coordination and the localized electron density, thereby inhibiting the oxidation of Sn^{2+}. *In situ* polymerization of polymer monomers in the perovskite films forms a polymer network that not only helps to bind the perovskite grains tightly, but also weaken coordination between polymer groups and the perovskite, resulting in a pinhole-free and passivated film, thereby improves the stability of the device.[122]

Device packaging is an important post-processing strategy to improve stability and serve as the most direct approach to inhibit film degradation. Moreover, effective packaging can accelerate the transition of perovskite FETs form the experimental stage to commercial applications. The conjugated polymer poly(3-hexylthiophene-2,5-diyl) (P3HT) is hydrophobic and protects the perovskite layers by preventing the diffusion of water molecules through the air. P3HT-encapsulated perovskite FETs exhibit a significant mobility compared with also popular Cytop-encapsulated perovskite FETs, which is attributed to the high capacitance polymer as a dielectric that can increase the induced charge carrier density.[65,123,124] In addition, conjugated polymers can effectively reduce the surface trap of perovskites by passivating the A-site cations and X-site anion defects.[123] In Nketia-Yawson's research work, the polymer encapsulation layer (P3HT) is processed through the orthogonal solvent, and the interface functionalization layer (IFL) can be formed on the top of the perovskites ($MAPbI_3$) without destroying the perovskite layers, and play the role of hydrophobic protection and interface defect passivation (Fig. 8d). The $MAPbI_3$/P3HT FETs with a perovskite-polymer hybrid channel can improve significantly mobility to 10.65 ± 0.84 cm^2 V^{-1} s^{-1} (pure P3HT with a mobility of 6.22 ± 1.87 cm^2 V^{-1} s^{-1}), and it has good air stability, with only a slight decline in transfer characteristics after 168 hours of exposure to air.[124] However, the hole mobility decreases with increasing thickness, possibly due to trapping of

holes in the perovskite channels and the perovskite/IFL interface, as well as increased resistance to charge transport in the vertical direction.

5.3 Ion migration and hysteresis effect

Fig. 9a describes the influence mechanism of ion migration on the performance of FET.[95] The mobile ions in the perovskite accumulated at the source/drain electrode, and the built-in electric field in the opposite direction is driven by the source and drain voltage, which hinders the transport of charge carriers. Moreover, the anion at the source and the cation at the drain cause the downward and upward band bending, respectively, thus increasing the carrier injection barrier or contact resistance, which adversely affects the performance of FETs. At the same time, these mobile ions in perovskite are also the origin of shallow defects, such as tin vacancy (V_{Sn}), lead vacancy (V_{Pb}), and iodine vacancy (V_I). Uncoordinated I^-, Sn^{2+}, Pb^{2+}, and oxidized Sn^{4+} accumulate at the interface, surface, and grain boundary, which are the main source of deep defects.[95] Shallow defect tin vacancies V_{Sn} in tin-based perovskites is taken as an example to understand the adverse effects of defects. As shown in Fig. 9b, free-falling holes get trapped in the negatively charged V_{Sn}, and hole de-trapping requires additional activation energy such as light or heat. It takes only a few microseconds for the carrier from getting trapped to de-trapped, but this process delays drift transmission and reduces the overall mobility of carriers. The tetrafluoro-tetracyanoquinodimethane (F4-TCNQ) and molybdenum trioxide (MoO_3) molecules are rich in electronegative atoms (F, N, and O), which exhibit strong electron withdrawing properties and can cause doping of p-type molecules,

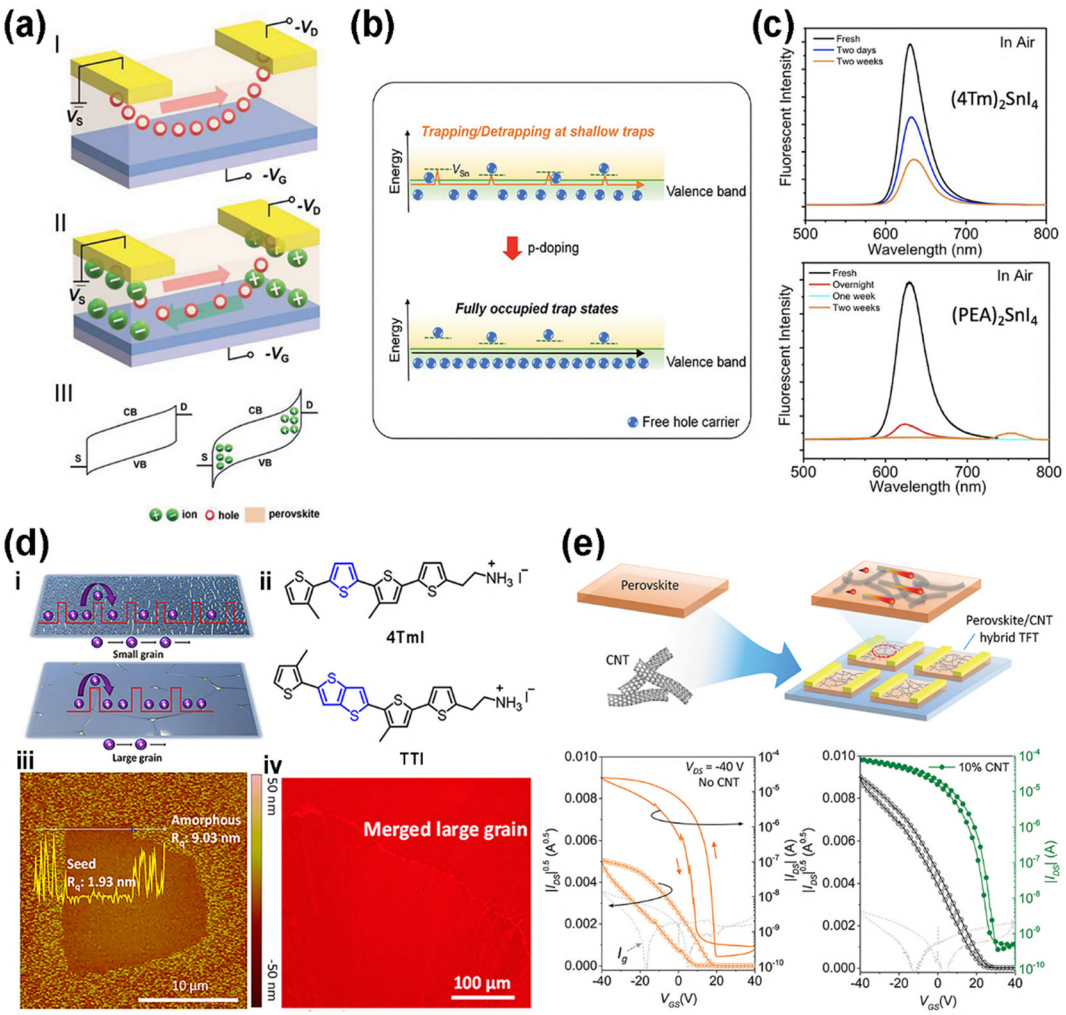

Fig. 9 (a) Schematic diagrams of the working mechanism of the $(PEA)_2SnI_4$ transistor without ion migration (I) and the Pb-containing perovskite transistors with ion migration (II), as well as the corresponding band bending at the source/drain electrodes (III).[95] (b) Schematic of the charge transport: charge trapping/de-trapping mechanism and occupation of trap states in pristine and doped-$(PEA)_2SnI_4$.[7] (c) Evolution of PL spectra of $(PEA)_2SnI_4$ and $(4Tm)_2SnI_4$ thin films in air.[91] (d) (i) Illustrations of carrier transport in small-grain and large-grain-based $(TT)_2SnI_4$ thin films. (ii) The chemical structures of 4TmI and TTI. (iii) AFM image and corresponding section analysis of a $(TT)_2SnI_4$ crystalline seed. (iv) PL image of the $(TT)_2SnI_4$ thin film.[92] (e) Schemes for $(PEA)_2SnI_4$/semi-CNT hybrid TFTs and TFT transfer characteristics with or without semi-CNT content at a scan rate of 1 V s^{-1}.[126] Figures reproduced with permission from: (a) ref. 95. Copyright 2021, Wiley-VCH GmbH; (b) ref. 7. Copyright 2022, Wiley-VCH GmbH; (c) ref. 91. Copyright 2019; (d) ref. 92. Copyright 2021, American Chemical Society; (e) ref. 126. Copyright 2019, American Chemical Society.

then the electrons in electron–hole pairs will be consumed and left free holes to achieve continued hole transport.[7] Besides, the defect state trap at the interface may cause abnormal negative difference resistance (NDR) phenomena in the output characteristic curve.[125]

Current–voltage hysteresis is a great challenge for FET devices to operate continuously at the same threshold voltage.[126] Sn^{2+} is mentioned in Section 3 as a source of hysteresis, because the accumulation of Sn^{2+} ions under bias reduces the number of holes in the channel by reducing the effective field strength of the gate or acting as a hole scattering center by coulomb repulsion, resulting in hysteresis.[12,88] Some charge transport layers, such as ZnO, while reducing the electron extraction barrier, can also adsorb oxygen molecules and capture electrons, making their surfaces negatively charged. When these trapped electrons combine with the photo-generated holes, oxygen will be released, resulting in the current hysteresis effect.[127] Other causes of hysteresis include prolonged voltage bias, defect-induced scattering, modulation of charge transport by trapping and de-trapping processes, and tunneling caused by heavy doping.[34,126] Moreover, in the top-contact device structure, the electrochemical reaction between the metal and the semiconductor will be detrimental to the stability of the device, such as the oxidation of Au in $MAPbBr_3$-based FETs ($3Br^- - 3e + Au \rightarrow AuBr_3$), which is verified by high-resolution XPS and time-of-flight secondary ion mass spectrometry.[77]

Recent advances have been focused on improving the stability of perovskite FETs, and many improvement strategies have been proposed in terms of crystal structure, film quality, grain boundary/defect passivation, processing technology, and so on. A large number of studies have indicated that introducing large aromatic or aliphatic organic cations into two-dimensional organo-inorganic hybrid perovskites is very critical to the environmental stability of perovskites. In particular, the bulky and hydrophobic conjugated ligands not only have advantages in regulating crystal structure but also have outstanding stability for perovskite films.[11,91,92] For example, $(4Tm)_2SnI_4$ thin film remained in the air for a month and maintained red photoluminescence, while $(PEA)_2SnI_4$ thin film degraded after only one night, and the PL spectra evolution of the two films in the air also confirmed this result (Fig. 9c). In general, ion migration at grain boundaries is faster, and small grains result in more grain boundaries, creating more defects and barriers for lateral charge transport (Fig. 9d-i). The reduction of grain boundaries leads to suppressed ion migration, alleviating hysteresis.[66] Compared with 4Tm molecule, the TT molecule structure shows a larger conjugated plane (Fig. 9d-ii), and introduction of fused thiophene rings in the organic ligand enhance the intermolecular interactions, thus $(TT)_2SnI_4$ thin film showed morphology with large grain size, and exhibited decent stability in both crystal structure and environment (Fig. 9d-iii and iv).[92] Moreover, optimizing the fabrication process is also an effective way to obtain large grain sizes. For organic ligands with larger molecular weight, increasing the annealing temperature is not only suitable for the recombination of organic and non-organic groups in the precursor but also helpful for increasing crystallinity and grain size.[91,92] When chlorobenzene is used as antisolvent, ethanol with a higher boiling point is added at the same time, the morphology of the film can be adjusted to obtain a high-quality film with a single grain size of 5 μm, and compared with pure chlorobenzene as antisolvent, the film has fewer pinholes and higher coverage. This is because the polar ethanol could dissolve the excess reactant precipitated upon the addition of chlorobenzene.[113,128] The binary solvent system, combined with chlorobenzene and ethyl acetate as the antisolvent in the spin-coating process, can promote nucleation and directional crystallization as well as improve the quality of the film, and ethyl acetate is relatively environmentally friendly.[129] Thermal spin coating is also an effective means to increase grain size, and its effect on the performance of FETs is the synergistic result of temperature and grain boundary.[130] The migration of defect-state ions is mainly concentrated at the grain boundary, which is inhibited at low temperatures and promoted at high temperatures. The thermal spin coating results in a large grain size and less influence of temperature on the properties. The roughness of the films annealed at low pressure is smaller, which is conducive to the reduction of the contact resistance between the semiconductor and the electrode.[131]

The embedded conjugated polymer-wrapped semiconducting carbon nanotubes (semi-CNTs) have a natural transmission channel, so coupling them with low-dimensional perovskite $(PEA)_2SnI_4$ is equivalent to opening up a "green channel" for carrier transmission, reducing the capture and scattering of carriers.[126] The results suggest that $(PEA)_2SnI_4$ doped with semi-CNTs has significantly reduced current–voltage sweep hysteresis and enhanced operational stability, and has the lowest trap density (2.06×10^{11} cm^{-2}) when the doping amount is 10% (Fig. 9e). The sorted single-wall carbon nanotubes (95% s-SWCNTs) doped into the mixed-perovskite $(MA_{1-x}FA_x)Pb(I_{1-x}Br_x)_3$ *via* a solution method can improve the on/off current ratio by four orders of magnitude (up to 10^7) compared to the unsorted ones, and the mobility is up to 32.25 cm^2 V^{-1} s^{-1}.[132] In addition, there are van der Waals and Coulomb force interactions among carbon nanotubes, the ionic components, and solvent molecules in the precursor solution, and the inherent dispersibility of the nanotubes makes the film uniform and continuous without pinholes. Thus, the reduction of defects and charge scattering results in an improved performance.

2D/3D perovskite films, prepared by mixing a small amount of 2D perovskites in 3D perovskites, generally exhibit better crystal orientation, resulting in higher crystallinity and improved stability. Moreover, 2D/3D perovskites appear to be less affected by grain boundaries and pinholes because charge transport primarily occurs in the inorganic octahedral layers between 3D grains near the substrate, and the electrical coupling between grains is sufficient to support carrier transport with little effect from pinholes.[133] For example, FPEA ligands are doped into 3D $FASnI_3$, and due to their large dipole moment, the resulting 2D/3D perovskite tends to grow parallel to the substrates. It enhances transverse carrier transport, resulting in significantly improved hole mobility (12 cm^2 V^{-1} s^{-1}) and on/

off current ratio ($>10^8$), with increased operational reliability and environmental stability.[134] Furthermore, a small amount of Cs is added based on FPEA to passivate defects and regulate ordered crystallization. The FETs with low-defect channel interfaces created by the three-cation project show high hole mobility (70 $cm^2\ V^{-1}\ s^{-1}$).[135]

Zhu and co-workers reported a series of common strategies for improving the performance and stability of transistors (Fig. 10a).[136] The first is the self-passivation strategy, that is, excess precursor components (*i.e.*, PEAI) are used to fill the grain boundaries, reducing the capture of charge carriers by defects. When the mole ratio of PEAI to SnI_2 reaches 2.4, the transfer characteristics of FETs are improved obviously (Fig. 10b). FPEAI was also introduced in Chao *et al.*'s study to self-passivate grain boundaries through surface recrystallization and improve stability significantly due to FPEAI's hydrophobicity more than PEAI's.[137] Self-passivation in this work also involves the addition of elemental tin powder to inhibit the oxidation of Sn^{2+} by the redox reaction. The same self-passivation strategy can also be accomplished with iodized metal salts. When the conventional annealed film is applied to further DMF solvent annealing, the residual MAI and PbI_2 will form MAI:PbI_2:DMF solvate with DMF, thus eliminating the adverse effects of PbI_2 accumulated at the grain boundaries, passivating the grain boundaries, reducing vacancy-mediated ion migration, and thus enhancing the charge transport.[62,138] The second is grain crystallization engineering. Different from the large grain size achieved by Gao *et al.* through regulating organic ligands, the focus of this work is to study the formation and decomposition of PEAI·SnI_2·Lewis-base (*i.e.*, DMSO, GBL, and NMP) intermediates during the crystallization process of perovskites.[91,92] Compared with DMSO, urea has a higher boiling point and larger dipole moment, which can better enhance the passivation effect of Lewis intermediate and promote grain growth.[139] Other research groups have also focused on the passivation of grains by solvents. The use of diethyl sulfide (DES) as an additive in the $MAPbI_3$ precursor can react with Pb^{2+} to form a strong intermediate chelate complex, and it is easier to obtain high crystallinity perovskite thin films with good environmental stability. At the same time, AlO_x with high capacitance as the dielectric layer can achieve stable operation at the low operating voltage, with an average saturation mobility of about 18.8 $cm^2\ V^{-1}\ s^{-1}$ (the highest measured value is 23 $cm^2\ V^{-1}\ s^{-1}$).[140] The solvent combination of DMF, DMSO, and HI is considered suitable for the formation of thin films in air. Among them, HI promotes uniform nucleation, DMF has a low boiling point and high vapor pressure, and the strong Lewis base property of DMSO can induce strong coordination with Pb^{2+}, which leads to rapid crystallization of the film and the formation of the large grain size.[116] The results show that the device performance in air is better than that in nitrogen, and it is speculated that water and oxygen in air also contribute significantly to defect passivation. The third is to use the passivation effect of trace oxygen on iodine vacancy to achieve p-doping, to improve the performance of $(PEA)_2SnI_4$ (p-channel) FETs. The charge density calculated by DFT sheds light on the mechanism of iodine vacancy passivation. The charge density is delocalized when there is an iodide vacancy defect, and localized when the iodide vacancy is occupied by oxygen molecules (Fig. 10c). Besides, reproducibility is also an important indicator for the fabrication of FET devices using the solution method, and it is closely related to every sub-process in the preparation process. Zhu *et al.* have reported a detailed and reproducible method for fabricating high-performance halogenated tin perovskite thin-film transistors based on solution engineering.[141] This approach provides an important tutorial manual for standardizing fabrication processes and effectively addresses reproducibility challenges.

6. Conclusions and perspectives

To sum up, we briefly introduce the working principle of FETs and the related physical properties of a halide perovskite

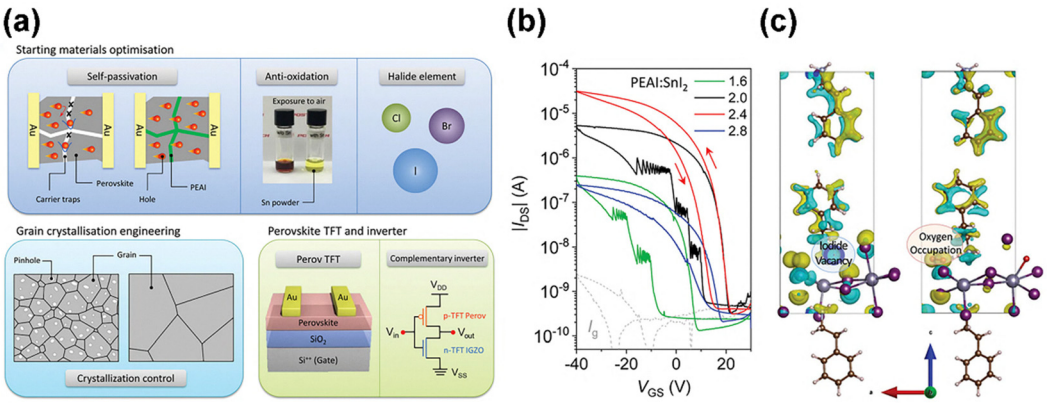

Fig. 10 (a) Schematic diagrams of self-passivation by adding slightly excess PEAI, anti-oxidation engineering by Sn powder, halide element effect, grain crystallization control by an adduct approach, and device. (b) Transfer characteristics of perovskite TFTs made from precursors with different mole ratios PEAI : SnI_2 = X : 1, X = 1.6, 2.0, 2.4, and 2.8, respectively (V_{DS} = −40 V). (c) Iodide vacancy and oxygen molecule occupying the iodide vacancy (isosurface level of 0.09).[136] Figures reproduced with permission from: ref. 136. Copyright 2020, Wiley-VCH GmbH.

transistor. The research progress of 2D/3D organic–inorganic hybrid halide perovskite FETs, including tin- and lead-based perovskite polycrystalline films or single-crystals, is reviewed. The factors affecting the performance of FETs are discussed in terms of ion migration, oxidative induced degradation, deep/shallow defects, current–voltage hysteresis, device parameter anomaly, electrochemical reaction of a semiconductor/electrode interface, *etc.* The general strategies of grain engineering, additive engineering, grain boundary passivation, defect passivation, mixed perovskite, and packaging technology to improve film quality and stability were summarized. Although basic issues such as low mobility, poor film quality, and the ability to operate at room temperature have been gradually improved, possibilities of improvement are further expected in the stable operation in air, applications of large areas and microelectronics, good reproducibility, control of crystallization dynamics, and excellent FET characteristics.

In organic and inorganic hybrid perovskites, especially the design of organic molecular ligands in 2D perovskite can diversify materials as well as achieve targeted device performance improvement. The emerging "OSiP", known as organic semiconductor-incorporated perovskites, offers vast opportunities for tailoring the energy landscape, carrier dynamics, and transport properties. Through the molecular engineering strategy of substituents and heteroatoms to control the ligand planarity, intra/intermolecular interaction, and energy level, it is expected to achieve the regulation of physical properties, processing properties, and carrier transport types. In general, applying conjugated organic molecules as ligands in 2D perovskites is conducive to construct large crystalline regions, so as to alleviate the capture of carriers by defects at the grain boundaries (Fig. 11a-i). Meanwhile, the large crystalline region is also a natural domain limited platform. The variation of the conjugated planes will also be reflected in HOMO/LUMO energy levels, and it is possible to achieve bipolar carrier transport when suitable energy level structures are deliberately designed. Introducing conjugated polymers is the most direct and effective way to increase the number of conjugated planes, but the polymer as an organic ligand has great challenges in either *in situ* polymerization or crystal structure integrity. Besides, the doping strategy applied in halide perovskites is very useful for the intentional engineering of carrier density, so most studies use the direct mixing method, which also seems to play a role in the passivation of grain boundaries. However, it is often confused with the passivation of additive engineering, making it difficult to truly understand the purpose of doping. Given this, it is meaningful to clarify the definition and method of doping in future research.[142]

Mixed-dimensional vertical heterojunction (such as 2D/3D and 1D/3D heterojunction) is a new method to combine the advantages of different dimensional perovskites without considering the phase distribution of low-dimensional perovskites

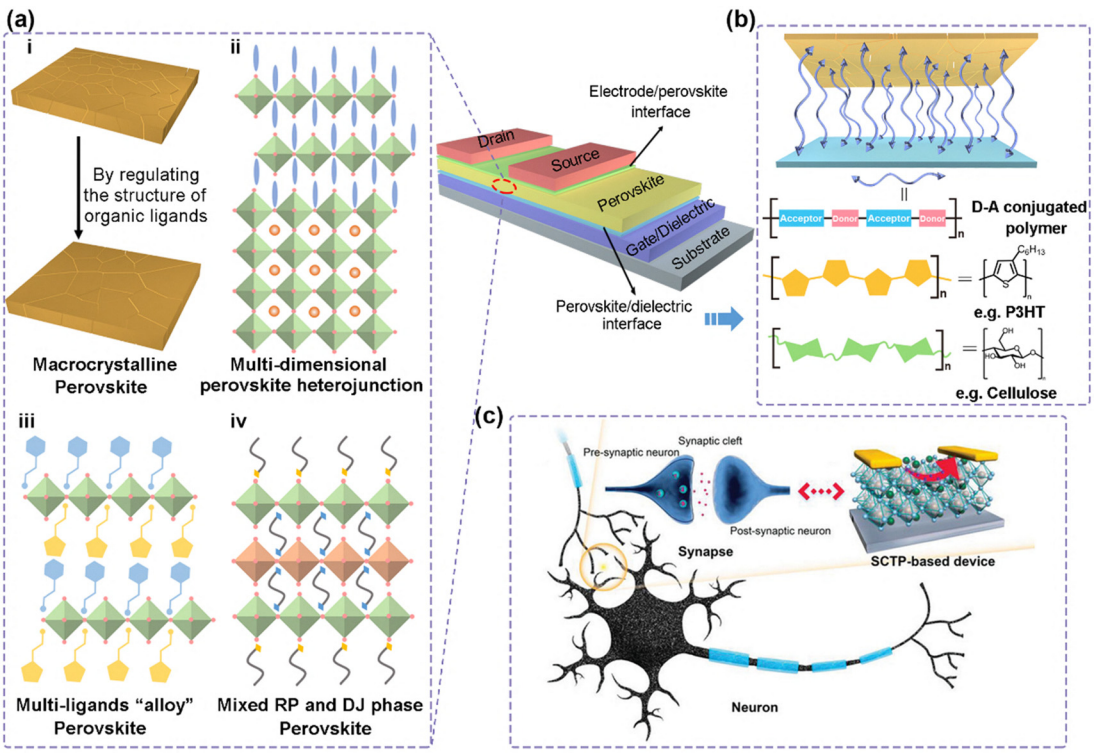

Fig. 11 Schematic diagram of optimization of high-quality perovskite thin film field-effect transistors. (a) The strategy of macrocrystalline perovskite regulated by organic ligands for (i), the strategy of multi-dimensional perovskite heterojunction for (ii), the strategy of multi-ligands "alloy" perovskite for (iii), and the strategy of mixed RP and DJ phase perovskite for (iv). (b) The strategy of passivation interface with polymers. (c) The potential application of perovskite FETs in artificial synapses.[146] Reproduced from ref. 146 with permission from the Wiley-VCH GmbH.

and has outstanding advantages in promoting ordered crystallization (Fig. 11a-ii). Inspired by the design philosophy of mixed halide perovskite $FA_{1-x-y}MA_xCs_yPbI_{3-z}Br_z$, we assume some ligand alloy systems on the basis of the structure of 2D perovskites could also bring some opportunities. For instance, the phenylethylamine in $(PEA)_2SnI_4$ is partially replaced by the thiophene ligand (thiophenethylamine) with a similar ligand length to form a new perovskite $(PEA_{1-x}TEA_x)_2SnI_4$, and the crystallization process is expected to be regulated by controlling the ligand content (Fig. 11a-iii). Realization of Janus structures in 2D perovskites is challenging yet worth trying using ligand alloy strategies. Mixed RP and DJ phase 2D perovskites are another possibility (Fig. 11a-iv), their energy level structure and bandgap can be adjusted *via* regulating the proportion between RP and DJ phase ligands. Compared with single RP or DJ phase perovskites, mixed phase perovskites have the advantages of both structures, showing better stability and higher carrier mobility.

For the preparation of high-quality perovskite field-effect transistors, it is not solely necessary to pay attention to the development and innovation of perovskite materials, but also to solve the contact problem between the semiconductor layer and the electrode or insulation layer. As mentioned above, the interface between the source/drain electrode and the semiconductor determines the carrier injection efficiency when the FET is operating, while the interface between the semiconductor layer and the insulator layer determines the carrier transmission performance. Modifying the source/drain surface could reduce the contact resistance through adjusting the electrode work function, meanwhile SAMs can help prevent electrochemical reactions at the electrode/perovskite interface upon biasing of the devices. However, in the process of source/drain interface modification, a problem that needs to be attended to is corrosion of electrodes, which also needs to be avoided. The optimization of the insulation layer interface is mainly to decrease the defect intensity, lessen the interface polarization, and induce ordered perovskite films. Polymers having abundant natural functional groups, good solution processing properties, are competitive candidates for promoting grain boundary healing and regulating crystallization (Fig. 11b). As an interface functionalized layer, conjugated polymers allow the use of a high-capacitance electrolyte dielectric in perovskite FETs, enabling excellent gate modulation with low driving voltages. Conjugated polymers can not only passivate interface defects, but also provide additional carrier transport pathways, or form a multi-dielectric layer structure to gain excellent dielectric performance and controllable film thickness.[124] We assume it is highly possible to realize high mobility as well as operational stability through interfacial functionalization of perovskites using conjugated polymers. Natural polymers like cellulose are rich, environmentally friendly, and low-cost. Due to its good mechanical properties and chemically inert nature, cellulose that can stabilize the crystal structure; its high toughness can resist crack growth; its rich functional groups can passivate defects; and its long chain has a good ability of grain boundary positioning. Therefore, using cellulose to optimize the interface is also a good choice. It also can contribute to the dielectric constant of the insulation layer.[143–145]

At the same time, the accurate extraction of mobility is also acritical challenge. The actual charge transport process is affected by complex factors, likely phonon scattering, ion migration, polarization disorder, hysteresis, contact resistance, and dynamic scattering, so the high mobilities reported in many reports are likely to be overestimated.[62] In the presence of large contact resistance, the inherent mobility can only be obtained at high voltage; therefore, to obtain accurate mobility, linear fitting should be performed at high voltage.[62] The mobility of a $MAPbBr_3$ single crystal FETs extracted by the transconductance method is 15 $cm^2\ V^{-1}\ s^{-1}$ (effective mobility is about 10 $cm^2\ V^{-1}\ s^{-1}$), and the confidence factor is about 88.7%.[77] In general, there are differences between μ_{lin} and μ_{sat} of the same device, and the μ_{lin} is lower than the true value, which may be related to the charge transfer involving the trap state.[147] The existence of hysteresis leads to a deviation in the calculation of mobility.[8] Therefore, the accurate extraction of mobility is of great significance to the evaluation of FET performance. Firstly, we need to define a standard that the expected carrier should be extracted when there is a linear relationship ($\sigma = \mu en$) between carrier density (n) and conductivity (σ), that is, both linear and saturated regions of the transfer characteristic curve need linear dependence, and it is inaccurate to extract mobility only in a very limited linear range.[148] Then, the following suggestions are made to improve the reliability of device mobility. The use of a vertical field effect transistor (VFET) may help reflect the intrinsic mobility because the vertical current is not dependent on the surface defect.[78] Moreover, this structure is conducive to realizing short-channel devices, increasing current density and the carrier extraction rate, and decreasing the carrier scattering rate.[149] The smoother surface of the film, the lower probability of carrier scattering, and the preparation of high-quality films is also the premise to ensure accurate mobility.[110] Reliability factor correction for non-ideal characteristics to obtain accurate mobility is recommended.[98] Moreover, the pattern processing is carried out to make the channel width and length close to the defined values, in order to eliminate the influence of redundant channels and fringe effect, so as to obtain the real carrier mobility.[150] If necessary, Hall effect measurements can also be performed to confirm estimated mobility values.

Halide perovskite FETs usually exhibit significant hysteresis, which may originate from ion migration, charge capture, and ferroelectric effects. Lots of efforts have been made to mitigate this phenomenon. Interestingly, the hysteretic behaviours become valuable properties for an artificial synapse, which require gradual modulation of responses, resembling flexible regulation of charge conductance and retention of synapse in neural networks (Fig. 11c). For example, the $(PEA)_2PbBr_4$/C8-BTBT heterojunction films displayed conversion of various synapse behaviours under electron or light stimulation.[151] The incorporation of $(PEA)_2PbBr_4$ induces trap states, resulting in the heterojunction FET displaying more significant anticlockwise hysteresis compared to the pristine C8-BTBT device. At

the same time, halide perovskites can provide efficient light signal perception and conversion capabilities for artificial synapses. Coupled with the rich material system and relatively simple preparation process of halide perovskites, we expect that the utilization of halide perovskite FETs for artificial synapses has a bright future.

Conflicts of interest

The authors declare no conflicts of interest.

Data availability

No primary research results, software or code have been included and no new data were generated or analysed as part of this review.

Acknowledgements

This work was financially supported by the National Natural Science Foundation of China (no. 22205070, 22475077, 92261204 and 22431005), the National Key R&D Program of China (2022YFB3807700), the Fundamental Research Funds for the Central Universities, South-Central Minzu University (CZQ24024), the Hubei Provincial Natural Science Foundation (no. 2023AFB421), and the Hubei Provincial Science and Technology Innovation Team Project (no. 2021CFA020 and 2024AFA012).

References

1 Y.-H. Lin, P. Pattanasattayavong and T. D. Anthopoulos, Metal-Halide Perovskite Transistors for Printed Electronics: Challenges and Opportunities, *Adv. Mater.*, 2017, **29**, 1702838.
2 A. Younis, C.-H. Lin, X. Guan, S. Shahrokhi, C.-Y. Huang, Y. Wang, T. He, S. Singh, L. Hu, J. R. D. Retamal, J.-H. He and T. Wu, Halide Perovskites: A New Era of Solution-Processed Electronics, *Adv. Mater.*, 2021, **33**, 2005000.
3 J. Sun, K. Wang, K. Ma, J. Y. Park, Z.-Y. Lin, B. M. Savoie and L. Dou, Emerging Two-Dimensional Organic Semiconductor-Incorporated Perovskites? A Fascinating Family of Hybrid Electronic Materials, *J. Am. Chem. Soc.*, 2023, **145**, 20694–20715.
4 S. Yang, J. Wen, Y. Wu, H. Zhu, A. Liu, Y. Hu, Y.-Y. Noh, J. Chu and W. Li, Unlocking the Potential of Tin-Based Perovskites: Properties, Progress, and Applications in New-Era Electronics, *Small*, 2024, **20**, 2304626.
5 A. Liu, H. Zhu, S. Bai, Y. Reo, M. Caironi, A. Petrozza, L. Dou and Y.-Y. Noh, High-Performance Metal Halide Perovskite Transistors, *Nat. Electron.*, 2023, **6**, 559–571.
6 T. H. Chowdhury, Y. Reo, A. R. B. M. Yusoff and Y.-Y. Noh, Sn-Based Perovskite Halides for Electronic Devices, *Adv. Sci.*, 2022, **9**, 2203749.
7 Y. Reo, H. Zhu, A. Liu and Y.-Y. Noh, Molecular Doping Enabling Mobility Boosting of 2D Sn^{2+}-Based Perovskites, *Adv. Funct. Mater.*, 2022, **32**, 2204870.
8 H. Shen, J. Li, H. Wang, J. Ma, J. Wang, H. Luo and D. Li, Two-Dimensional Lead-Free Perovskite $(C_6H_5C_2H_4NH_3)_2CsSn_2I_7$ with High Hole Mobility, *J. Phys. Chem. Lett.*, 2019, **10**, 7–12.
9 C. Chen, X. Zhang, G. Wu, H. Li and H. Chen, Visible-Light Ultrasensitive Solution-Prepared Layered Organic-Inorganic Hybrid Perovskite Field-Effect Transistor, *Adv. Opt. Mater.*, 2017, **5**, 1600539.
10 J.-H. Cho, J.-Y. Go, T. T. Bui, S. Mun, Y. Kim, K. Ahn, Y.-Y. Noh and M.-G. Kim, Anion-Vacancy-Defect Passivation of a 2D-Layered Tin-Based Perovskite Thin-Film Transistor with Sulfur Doping, *Adv. Electron. Mater.*, 2022, **9**, 2201014.
11 Y. Gao, E. Shi, S. Deng, S. B. Shiring, J. M. Snaider, C. Liang, B. Yuan, R. Song, S. M. Janke, A. Liebman-Pelaez, P. Yoo, M. Zeller, B. W. Boudouris, P. Liao, C. Zhu, V. Blum, Y. Yu, B. M. Savoie, L. Huang and L. Dou, Molecular Engineering of Organic-Inorganic Hybrid Perovskites Quantum Wells, *Nat. Chem.*, 2019, **11**, 1151–1157.
12 T. Matsushima, T. Yasuda, K. Fujita and C. Adachi, Field-Effect Transistors with Vacuum-Deposited Organic-Inorganic Perovskite Films as Semiconductor Channels, *J. Appl. Phys.*, 2016, **120**, 233301.
13 N. Guo, J. Li, S. Yang, J. Zhang, J. Ni and H. Cai, Dimensional Structure Regulation of Organic-Inorganic Hybrid Perovskite and Its Application in Thin Film Transistors, *Nanotechnology*, 2021, **32**, 395704.
14 T. Matsushima, S. Hwang, S. Terakawa, T. Fujihara, A. S. D. Sandanayaka, C. Qin and C. Adachi, Intrinsic Carrier Transport Properties of Solution-Processed Organic-Inorganic Perovskite Films, *Appl. Phys. Express*, 2017, **10**, 024103.
15 B. He, W. Li, Q. Wang, L. Liang, H. Wang, J. Xu, S. Yang, Y. Jiang, Y. Tang and B. Zou, Ultrasensitive All-Solution-Processed Field-Effect Transistor Based Perovskite Photodetectors with Sol-Gel SiO_2 as the Dielectric Layer, *J. Alloys Compd.*, 2017, **717**, 150–155.
16 J.-K. Huang, Y. Wan, J. Shi, J. Zhang, Z. Wang, W. Wang, N. Yang, Y. Liu, C.-H. Lin, X. Guan, L. Hu, Z.-L. Yang, B.-C. Huang, Y.-P. Chiu, J. Yang, V. Tung, D. Wang, K. Kalantar-Zadeh, T. Wu, X. Zu, L. Qiao, L.-J. Li and S. Li, High-Kappa Perovskite Membranes as Insulators for Two-Dimensional Transistors, *Nature*, 2022, **605**, 262–267.
17 J. Guo, Y. Liu, P.-A. Chen, X. Qiu, H. Wei, J. Xia, H. Chen, Z. Zeng, L. Liao and Y. Hu, Tuning the Electrical Performance of 2D Perovskite Field-Effect Transistors by Forming Organic Semiconductor/Perovskite van der Waals Heterojunctions, *Adv. Electron. Mater.*, 2022, **8**, 2200148.
18 Y. Liang, F. Li and R. Zheng, Low-Dimensional Hybrid Perovskites for Field-Effect Transistors with Improved Stability: Progress and Challenges, *Adv. Electron. Mater.*, 2020, **6**, 2000137.
19 A. R. B. M. Yusoff, H. P. Kim, X. Li, J. Kim, J. Jang and M. K. Nazeeruddin, Ambipolar Triple Cation Perovskite

Field Effect Transistors and Inverters, *Adv. Mater.*, 2017, **29**, 1602940.
20 L. Li, X. Liu, J. Guo, H. Ji, F. Zhang, Z. Lou, L. Qin, Y. Hu, Y. Hou and F. Teng, Low-Operating-Voltage Two-Dimensional Tin Perovskite Field-Effect Transistors with Multilayer Gate Dielectrics Based on a Fluorinated Copolymer, *J. Phys. Chem. Lett.*, 2023, **14**, 2223–2233.
21 J. W. Ward, H. L. Smith, A. Zeidell, P. J. Diemer, S. R. Baker, H. Lee, M. M. Payne, J. E. Anthony, M. Guthold and O. D. Jurchescu, Solution-Processed Organic and Halide Perovskite Transistors on Hydrophobic Surfaces, *ACS Appl. Mater. Interfaces*, 2017, **9**, 18120–18126.
22 F. Zhang, H. Zhang, L. Zhu, L. Qin, Y. Wang, Y. Hu, Z. Lou, Y. Hou and F. Teng, Two-Dimensional Organic-Inorganic Hybrid Perovskite Field-Effect Transistors with Polymers as Bottom-Gate Dielectrics, *J. Mater. Chem. C*, 2019, **7**, 4004–4012.
23 J. Kim, Y.-S. Shiah, K. Sim, S. Iimura, K. Abe, M. Tsuji, M. Sasase and H. Hosono, High-Performance P-Channel Tin Halide Perovskite Thin Film Transistor Utilizing a 2D-3D Core-Shell Structure, *Adv. Sci.*, 2022, **9**, 2104993.
24 S. Wang, Z. Ling, P. W. M. Blom, T. Marszalek and W. Pisula, Engineering Strategies for 2D Layered Tin Halide Perovskite Field-Effect Transistors, *Adv. Funct. Mater.*, 2025, 2501217.
25 T. Zou and Y.-Y. Noh, Solution-Processed 2D Transition Metal Dichalcogenides: Materials to Cmos Electronics, *Acc. Mater. Res.*, 2023, **4**, 548–559.
26 A. J. Yang, S.-X. Wang, J. Xu, X. J. Loh, Q. Zhu and X. R. Wang, Two-Dimensional Layered Materials Meet Perovskite Oxides: A Combination for High-Performance Electronic Devices, *ACS Nano*, 2023, **17**, 9748–9762.
27 B. Zheng and L. Huo, Recent Advances of Dithienobenzodithiophene-Based Organic Semiconductors for Organic Electronics, *Sci. China:Chem.*, 2021, **64**, 358–384.
28 A. Chougle, A. Rezk, S. U. Bin Afzal, A. K. Mohammed, D. Shetty and A. Nayfeh, Evolving Role of Conjugated Polymers in Nanoelectronics and Photonics, *Nano-Micro Lett.*, 2025, **17**, 230.
29 T. Wu, W. Pisula, M. Y. Abd Rashid and P. Gao, Application of Perovskite-Structured Materials in Field-Effect Transistors, *Adv. Electron. Mater.*, 2019, **5**, 1900444.
30 W. Yang, L. Dou, H. Zhu and Y.-Y. Noh, Ruddlesden-Popper Tin-Based Halide Perovskite Field-Effect Transistors, *Small Struct.*, 2024, **5**, 2300393.
31 F. Zhang, Q. Zhang, X. Liu, L. Qin, Y. Hu, Z. Lou, Y. Hou and F. Teng, Ambipolar Transport in Two-Dimensional Sn-Based Perovskite Field-Effect Transistors Using an Aliphatic Polymer-Assisted Method, *J. Mater. Chem. A*, 2021, **9**, 22842–22853.
32 J. Zaumseil and H. Sirringhaus, Electron and Ambipolar Transport in Organic Field-Effect Transistors, *Chem. Rev.*, 2007, **107**, 1296–1323.
33 J. Wang, F. Liu, G. Wang, L. Wang and C. Jiang, Novel Organic-Perovskite Hybrid Structure Forward Photo Field Effect Transistor, *Org. Electron.*, 2016, **38**, 158–163.
34 T. Matsushima, F. Mathevet, B. Heinrich, S. Terakawa, T. Fujihara, C. Qin, A. S. D. Sandanayaka, J.-C. Ribierre and C. Adachi, N-Channel Field-Effect Transistors with an Organic-Inorganic Layered Perovskite Semiconductor, *Appl. Phys. Lett.*, 2016, **109**, 253301.
35 Z. Wei, K. Wang, W. Zhao, Y. Gao, Q. Hu, K. Chen and L. Dou, A Selenophene-Containing Conjugated Organic Ligand for Two-Dimensional Halide Perovskites, *Chem. Commun.*, 2021, **57**, 11469–11472.
36 I. Chung, J.-H. Song, J. Im, J. Androulakis, C. D. Malliakas, H. Li, A. J. Freeman, J. T. Kenney and M. G. Kanatzidis, $CsSnI_3$: Semiconductor or Metal? High Electrical Conductivity and Strong Near-Infrared Photoluminescence from a Single Material. High Hole Mobility and Phase-Transitions, *J. Am. Chem. Soc.*, 2012, **134**, 8579–8587.
37 A. Liu, H. Zhu, S. Bai, Y. Reo, T. Zou, M.-G. Kim and Y.-Y. Noh, High-Performance Inorganic Metal Halide Perovskite Transistors, *Nat. Electron.*, 2022, **5**, 78–83.
38 A. Liu, H. Zhu, S. Kim, Y. Reo, Y.-S. Kim, S. Bai and Y.-Y. Noh, Antimony Fluoride (SbF_3): A Potent Hole Suppressor for Tin(II)-Halide Perovskite Devices, *InfoMat*, 2023, **5**, e12386.
39 C. Huo, X. Liu, X. Song, Z. Wang and H. Zeng, Field-Effect Transistors Based on Van-Der-Waals-Grown and Dry-Transferred All-Inorganic Perovskite Ultrathin Platelets, *J. Phys. Chem. Lett.*, 2017, **8**, 4785–4792.
40 J. Liu, F. Liu, H. Liu, R. Hou, J. Yue, J. Cai, Z. Peng, J. Impundu, L. Xie, Y. J. Li and L. Sun, Direct Growth of Perovskite Crystals on Metallic Electrodes for High-Performance Electronic and Optoelectronic Devices, *Small*, 2020, **16**, 1906185.
41 V. Bruevich, L. Kasaei, S. Rangan, H. Hijazi, Z. Zhang, T. Emge, E. Y. Andrei, R. A. Bartynski, L. C. Feldman and V. Podzorov, Intrinsic (Trap-Free) Transistors Based on Epitaxial Single-Crystal Perovskites, *Adv. Mater.*, 2022, **34**, 2205055.
42 C. C. Stoumpos, C. D. Malliakas and M. G. Kanatzidis, Semiconducting Tin and Lead Iodide Perovskites with Organic Cations: Phase Transitions, High Mobilities, and Near-Infrared Photoluminescent Properties, *Inorg. Chem.*, 2013, **52**, 9019–9038.
43 A. N. Aleshin, I. P. Shcherbakov, E. V. Gushchina, L. B. Matyushkin and V. A. Moshnikov, Solution-Processed Field-Effect Transistors Based on Polyfluorene Ecesium Lead Halide Nanocrystals Composite Films with Small Hysteresis of Output and Transfer Characteristics, *Org. Electron.*, 2017, **50**, 213–219.
44 Y. J. Lee, J. S. Han, D. E. Lee, T. H. Lee, J. Y. Kim, J. M. Suh, J. H. Lee, I. H. Im, S. J. Kim, K. J. Kwak and H. W. Jang, High Hole Mobility Inorganic Halide Perovskite Field-Effect Transistors with Enhanced Phase Stability and Interfacial Defect Tolerance, *Adv. Electron. Mater.*, 2022, **8**, 2100624.
45 Y. Chen, X. Wu, Y. Chu, J. Zhou, B. Zhou and J. Huang, Hybrid Field-Effect Transistors and Photodetectors Based on Organic Semiconductor and $CsPbI_3$ Perovskite Nanorods Bilayer Structure, *Nano-Micro Lett.*, 2018, **10**, 57.
46 X. Y. Chin, D. Cortecchia, J. Yin, A. Bruno and C. Soci, Lead Iodide Perovskite Light-Emitting Field-Effect Transistor, *Nat. Commun.*, 2015, **6**, 7383.

47 C. Eames, J. M. Frost, P. R. F. Barnes, B. C. O'Regan, A. Walsh and M. S. Islam, Ionic Transport in Hybrid Lead Iodide Perovskite Solar Cells, *Nat. Commun.*, 2015, **6**, 7497.
48 S. P. Senanayak, M. Abdi-Jalebi, V. S. Kamboj, R. Carey, R. Shivanna, T. Tian, G. Schweicher, J. Wang, N. Giesbrecht, D. Di Nuzzo, H. E. Beere, P. Docampo, D. A. Ritchie, D. Fairen-Jimenez, R. H. Friend and H. Sirringhaus, A General Approach for Hysteresis-Free, Operationally Stable Metal Halide Perovskite Field-Effect Transistors, *Sci. Adv.*, 2020, **6**, eaaz4948.
49 F. Maddalena, X. Y. Chin, D. Cortecchia, A. Bruno and C. Soci, Brightness Enhancement in Pulsed-Operated Perovskite Light-Emitting Transistors, *ACS Appl. Mater. Interfaces*, 2018, **10**, 37316–37325.
50 K. Hong, J. M. Kim, K. G. Cho, W.-S. Choi, J. Y. Park, J. Ham, J.-L. Lee and K. H. Lee, Solution-Processed Perovskite Gate Insulator for Sub-2 V Electrolyte-Gated Transistors, *J. Phys. Chem. C*, 2018, **122**, 10552–10558.
51 J. G. Labram, D. H. Fabini, E. E. Perry, A. J. Lehner, H. Wang, A. M. Glaudell, G. Wu, H. Evans, D. Buck, R. Cotta, L. Echegoyen, F. Wudl, R. Seshadri and M. L. Chabinyc, Temperature-Dependent Polarization in Field-Effect Transport and Photovoltaic Measurements of Methylammonium Lead Iodide, *J. Phys. Chem. Lett.*, 2015, **6**, 3565–3571.
52 M. Chen, X. Shan, T. Geske, J. Li and Z. Yu, Manipulating Ion Migration for Highly Stable Light-Emitting Diodes with Single-Crystalline Organometal Halide Perovskite Microplatelets, *ACS Nano*, 2017, **11**, 6312–6318.
53 J. H. L. Ngai, J. K. W. Ho, R. K. H. Chan, S. H. Cheung, L. M. Leung and S. K. So, Growth, Characterization, and Thin Film Transistor Application of $CH_3NH_3PbI_3$ Perovskite on Polymeric Gate Dielectric Layers, *RSC Adv.*, 2017, **7**, 49353–49360.
54 J. Xia, X. Qiu, Y. Liu, P.-A. Chen, J. Guo, H. Wei, J. Ding, H. Xie, Y. Lv, F. Li, W. Li, L. Liao and Y. Hu, Ferroelectric Wide-Bandgap Metal Halide Perovskite Field-Effect Transistors: Toward Transparent Electronics, *Adv. Sci.*, 2023, **10**, 2300133.
55 B. Jeong, L. Veith, T. J. A. M. Smolders, M. J. Wolf and K. Asadi, Room-Temperature Halide Perovskite Field-Effect Transistors by Ion Transport Mitigation, *Adv. Mater.*, 2021, **33**, 2100486.
56 B. Jeong, P. Gkoupidenis and K. Asadi, Solution-Processed Perovskite Field-Effect Transistor Artificial Synapses, *Adv. Mater.*, 2021, **33**, 2104034.
57 W. Xu, H. Cho, Y.-H. Kim, Y.-T. Kim, C. Wolf, C.-G. Park and T.-W. Lee, Organometal Halide Perovskite Artificial Synapses, *Adv. Mater.*, 2016, **28**, 5916–5922.
58 T. Roh, H. Zhu, W. Yang, A. Liu and Y.-Y. Noh, Ion Migration Induced Unusual Charge Transport in Tin Halide Perovskites, *ACS Energy Lett.*, 2023, **8**, 957–962.
59 J. H. Heo, S. H. Im, J. H. Noh, T. N. Mandal, C.-S. Lim, J. A. Chang, Y. H. Lee, H.-J. Kim, A. Sarkar, M. K. Nazeeruddin, M. Graetzel and S. I. Seok, Efficient Inorganic-Organic Hybrid Heterojunction Solar Cells Containing Perovskite Compound and Polymeric Hole Conductors, *Nat. Photonics*, 2013, **7**, 487–492.
60 H. Yu, Y. Cheng, D. Shin, S.-W. Tsang and F. So, Vertical Organic-Inorganic Hybrid Perovskite Schottky Junction Transistors, *Adv. Electron. Mater.*, 2018, **4**, 1800039.
61 F. Li, C. Ma, H. Wang, W. Hu, W. Yu, A. D. Sheikh and T. Wu, Ambipolar Solution-Processed Hybrid Perovskite Phototransistors, *Nat. Commun.*, 2015, **6**, 8238.
62 A. M. Zeidell, C. Tyznik, L. Jennings, C. Zhang, H. Lee, M. Guthold, Z. V. Vardeny and O. D. Jurchescu, Enhanced Charge Transport in Hybrid Perovskite Field-Effect Transistors Via Microstructure Control, *Adv. Electron. Mater.*, 2018, **4**, 1800316.
63 H. Zhu, A. Liu, K. I. Shim, H. Jung, T. Zou, Y. Reo, H. Kim, J. W. Han, Y. Chen, H. Y. Chu, J. H. Lim, H.-J. Kim, S. Bai and Y.-Y. Noh, High-Performance Hysteresis-Free Perovskite Transistors through Anion Engineering, *Nat. Commun.*, 2022, **13**, 1741.
64 Y. Kim, J. Kim, H. Ko and B. Park, The Formation of a Functional Pentacene/$CH_3NH_3PbI_{3-x}Cl_x$ Perovskite Interface: Optical Gating and Field-Induced Charge Retention, *Nanoscale*, 2018, **10**, 19383–19389.
65 V. Nketia-Yawson, B. Nketia-Yawson and J. W. Jo, High-Mobility Electrolyte-Gated Perovskite Transistors on Flexible Plastic Substrate Via Interface and Composition Engineering, *Appl. Surf. Sci.*, 2023, **623**, 156984.
66 N. D. Canicoba, N. Zagni, F. Liu, G. McCuistian, K. Fernando, H. Bellezza, B. Traore, R. Rogel, H. Tsai, L. Le Brizoual, W. Nie, J. J. Crochet, S. Tretiak, C. Katan, J. Even, M. G. Kanatzidis, B. W. Alphenaar, J.-C. Blancon, M. A. Alam and A. D. Mohite, Halide Perovskite High-K Field Effect Transistors with Dynamically Reconfigurable Ambipolarity, *ACS Mater. Lett.*, 2019, **1**, 633–640.
67 Z. Zhou, Q. Li, M. Chen, X. Zheng, X. Wu, X. Lu, S. Tao and N. Zhao, High-Mobility and Bias-Stable Field-Effect Transistors Based on Lead-Free Formamidinium Tin Iodide Perovskites, *ACS Energy Lett.*, 2023, **8**, 4496–4505.
68 W. Yang, K. Zhang, W. Yuan, L. Zhang, C. Qin and H. Wang, Enhancing Stability and Performance in Tin-Based Perovskite Field-Effect Transistors through Hydrogen Bond Suppression of Organic Cation Migration, *Adv. Mater.*, 2024, **36**, 2313461.
69 X. Yang, Y. Liu, S. Yang, Y. Wu, Y. Lei, Y. Yang, A. Liu, J. Chu and W. Li, High-Performance Tin-Halide Perovskite Transistors Enabled by Multiple A-Cation Engineering, *Adv. Funct. Mater.*, 2024, 2403917.
70 Y. Wang, C. Chen, T. Zou, L. Yan, C. Liu, X. Du, S. Zhang and H. Zhou, Spin-On-Patterning of Sn-Pb Perovskite Photodiodes on IGZO Transistor Arrays for Fast Active-Matrix Near-Infrared Imaging, *Adv. Mater. Technol.*, 2020, **5**, 1900752.
71 S. P. Senanayak, K. Dey, R. Shivanna, W. Li, D. Ghosh, Y. Zhang, B. Roose, S. J. Zelewski, Z. Andaji-Garmaroudi, W. Wood, N. Tiwale, J. L. MacManus-Driscoll, R. H. Friend, S. D. Stranks and H. Sirringhaus, Charge Transport in Mixed Metal Halide Perovskite Semiconductors, *Nat. Mater.*, 2023, **22**, 216–224.

72 D. Shin, M. Lai, Y. Shin, J. S. Du, L. Jibril, J. M. Rondinelli and C. A. Mirkin, From Heterostructures to Solid-Solutions: Structural Tunability in Mixed Halide Perovskites, *Adv. Mater.*, 2023, **35**, 2205923.

73 M. Klein, J. Li, A. Bruno and C. Soci, Co-Evaporated Perovskite Light-Emitting Transistor Operating at Room Temperature, *Adv. Electron. Mater.*, 2021, **7**, 2100403.

74 Y. Wu, J. Li, J. Xu, Y. Du, L. Huang, J. Ni, H. Cai and J. Zhang, Organic-Inorganic Hybrid $CH_3NH_3PbI_3$ Perovskite Materials as Channels in Thin-Film Field-Effect Transistors, *RSC Adv.*, 2016, **6**, 16243–16249.

75 G. Wang, D. Li, H.-C. Cheng, Y. Li, C.-Y. Chen, A. Yin, Z. Zhao, Z. Lin, H. Wu, Q. He, M. Ding, Y. Liu, Y. Huang and X. Duan, Wafer-Scale Growth of Large Arrays of Perovskite Microplate Crystals for Functional Electronics and Optoelectronics, *Sci. Adv.*, 2015, **1**, e150061.

76 W. Yu, F. Li, L. Yu, M. R. Niazi, Y. Zou, D. Corzo, A. Basu, C. Ma, S. Dey, M. L. Tietze, U. Buttner, X. Wang, Z. Wang, M. N. Hedhili, C. Guo, T. Wu and A. Amassian, Single Crystal Hybrid Perovskite Field-Effect Transistors, *Nat. Commun.*, 2018, **9**, 5354.

77 J. Wang, S. P. Senanayak, J. Liu, Y. Hu, Y. Shi, Z. Li, C. Zhang, B. Yang, L. Jiang, D. Di, A. V. Ievlev, O. S. Ovchinnikova, T. Ding, H. Deng, L. Tang, Y. Guo, J. Wang, K. Xiao, D. Venkateshvaran, L. Jiang, D. Zhu and H. Sirringhaus, Investigation of Electrode Electrochemical Reactions in $CH_3NH_3PbBr_3$ Perovskite Single-Crystal Field-Effect Transistors, *Adv. Mater.*, 2019, **31**, 1902618.

78 Y. Zou, Y. Shi, B. Wang, M. Liu, J. An, N. Zhang, L. Qi, W. Yu, D. Li and S. Li, Electrical and Optoelectrical Dual-Modulation in Perovskite-Based Vertical Field-Effect Transistors, *ACS Photonics*, 2022, **10**, 2280–2289.

79 S. P. Senanayak, B. Yang, T. H. Thomas, N. Giesbrecht, W. Huang, E. Gann, B. Nair, K. Goedel, S. Guha, X. Moya, C. R. McNeill, P. Docampo, A. Sadhanala, R. H. Friend and H. Sirringhaus, Understanding Charge Transport in Lead Iodide Perovskite Thin-Film Field-Effect Transistors, *Sci. Adv.*, 2017, **3**, e1601935.

80 X. Qiu, J. Xia, Y. Liu, P.-A. Chen, L. Huang, H. Wei, J. Ding, Z. Gong, X. Zeng, C. Peng, C. Chen, X. Wang, L. Jiang, L. Liao and Y. Hu, Ambient-Stable 2D Dion-Jacobson Phase Tin Halide Perovskite Field-Effect Transistors with Mobility over 1.6 $Cm^2\ V^{-1}\ S^{-1}$, *Adv. Mater.*, 2023, **35**, 2305648.

81 X. Li, J. M. Hoffman and M. G. Kanatzidis, The 2D Halide Perovskite Rulebook: How the Spacer Influences Everything from the Structure to Optoelectronic Device Efficiency, *Chem. Rev.*, 2021, **121**, 2230–2291.

82 C. R. Kagan, D. B. Mitzi and C. D. Dimitrakopoulos, Organic-Inorganic Hybrid Materials as Semiconducting Channels in Thin-Film Field-Effect Transistors, *Science*, 1999, **286**, 945–947.

83 D. B. Mitzi, C. D. Dimitrakopoulos and L. L. Kosbar, Structurally Tailored Organic-Inorganic Perovskites: Optical Properties and Solution-Processed Channel Materials for Thin-Film Transistors, *Chem. Mater.*, 2001, **13**, 3728–3740.

84 T. Matsushima, K. Fujita and T. Tsutsui, High Field-Effect Hole Mobility in Organic-Inorganic Hybrid Thin Films Prepared by Vacuum Vapor Deposition Technique, *Jpn. J. Appl. Phys.*, 2004, **43**, 1199–1201.

85 D. B. Mitzi, C. D. Dimitrakopoulos, J. Rosner, D. R. Medeiros, Z. T. Xu and C. Noyan, Hybrid Field-Effect Transistor Based on a Low-Temperature Melt-Processed Channel Layer, *Adv. Mater.*, 2002, **14**, 1772–1776.

86 H. Ryu, Y. Reo, W. Park, D. Lee, H. Choi, S. Yoo, A. Liu, H. Zhu and Y.-Y. Noh, Chloride Additives as Crystallinity Modulators in 2D Tin Halide Perovskite Transistors, *Small Struct.*, 2025, 2500055.

87 Y. Reo, T. Choi, J.-Y. Go, S. Jeon, B. Lim, H. Zhu, A. Liu and Y.-Y. Noh, Precursor Solution Aging: A Universal Strategy Modulating Crystallization of Two-Dimensional Tin Halide Perovskite Films, *ACS Energy Lett.*, 2023, **8**, 3088–3094.

88 T. Matsushima, S. Hwang, A. S. D. Sandanayaka, C. Qin, S. Terakawa, T. Fujihara, M. Yahiro and C. Adachi, Solution-Processed Organic-Inorganic Perovskite Field-Effect Transistors with High Hole Mobilities, *Adv. Mater.*, 2016, **28**, 10275–10281.

89 Y. Cai, S. Yan, X. Du, T. Lin, Y.-J. Lin, L. Qiu and W. Wang, 2D-Layered Manganese Perovskite with High Mobility, *Adv. Funct. Mater.*, 2023, **33**, 2211191.

90 S. Hu, B. Tang, S. V. Kershaw and A. L. Rogach, Metal Halide Perovskite Photo-Field-Effect Transistors with Chiral Selectivity, *ACS Appl. Mater. Interfaces*, 2023, **15**, 27307–27315.

91 Y. Gao, Z. Wei, P. Yoo, E. Shi, M. Zeller, C. Zhu, P. Liao and L. Dou, Highly Stable Lead-Free Perovskite Field-Effect Transistors Incorporating Linear Π-Conjugated Organic Ligands, *J. Am. Chem. Soc.*, 2019, **141**, 15577–15585.

92 A. Liang, Y. Gao, R. Asadpour, Z. Wei, B. P. Finkenauer, L. Jin, J. Yang, K. Wang, K. Chen, P. Liao, C. Zhu, L. Huang, B. W. Boudouris, M. A. Alam and L. Dou, Ligand-Driven Grain Engineering of High Mobility Two-Dimensional Perovskite Thin-Film Transistors, *J. Am. Chem. Soc.*, 2021, **143**, 15215–15223.

93 F. Zhang, M. Shao, C. Wang, W. Wen, W. Shi, M. Qin, H. Huang, X. Wei, Y. Guo and Y. Liu, Photoinduced Nonvolatile Memory Transistor Based on Lead-Free Perovskite Incorporating Fused Π-Conjugated Organic Ligands, *Adv. Mater.*, 2024, **36**, 2307326.

94 X. Liu, H. Ji, L. Li, F. Zhang, J. Guo, L. Qin, Z. Lou, D. Li, Y. Hu, Y. Hou and F. Teng, Two-Dimensional Layered Simple Aliphatic Monoammonium Tin Perovskite Thin Films and Potential Applications in Field-Effect Transistors, *ACS Appl. Mater. Interfaces*, 2022, **14**, 50401–50413.

95 C. Qin, F. Zhang, L. Qin, X. Liu, H. Ji, L. Li, Y. Hu, Z. Lou, Y. Hou and F. Teng, Charge Transport in 2D Layered Mixed Sn-Pb Perovskite Thin Films for Field-Effect Transistors, *Adv. Electron. Mater.*, 2021, **7**, 2100384.

96 X. Qiu, Y. Liu, J. Xia, J. Guo, P.-A. Chen, H. Wei, X. Shi, C. Chen, Z. Zeng, H. Chen, L. Jiang, L. Liao and Y. Hu, Room Temperature Two-Dimensional Lead Halide Perovskite Thin-Film Transistors with High Stability, *Cell Rep. Phys. Sci.*, 2023, **4**, 101217.

97 D. Liu, K. Liu and R. Quhe, Quantum Transport Simulations of a Monolayer All-Inorganic Perovskite Transistor, *J. Phys. D:Appl. Phys.*, 2020, **53**, 455104.
98 M. U. Chaudhry, N. Wang, K. Tetzner, A. Seitkhan, Y. Miao, Y. Sun, M. C. Petty, T. D. Anthopoulos, J. Wang and D. D. C. Bradley, Light-Emitting Transistors Based on Solution-Processed Heterostructures of Self-Organized Multiple-Quantum-Well Perovskite and Metal-Oxide Semiconductors, *Adv. Electron. Mater.*, 2019, **5**, 1800985.
99 H. Ji, X. Liu, L. Li, F. Zhang, L. Qin, Z. Lou, D. Li, Y. Hu, Y. Hou and F. Teng, Two-Dimensional Layered Dion-Jacobson Phase Organic-Inorganic Tin Iodide Perovskite Field-Effect Transistors, *J. Mater. Chem. A*, 2023, **11**, 7767–7779.
100 W. Park, M. Kwon, D. H. Lee, S. Yoo, W. Yang, J.-S. Park, A. Liu, Y. Reo, H. Zhu and Y.-Y. Noh, Odd-Even Effects of Linear Alkyl-Based Organic Spacers for Efficient Charge Transport in Two-Dimensional Dion-Jacobson Tin Perovskites, *J. Am. Chem. Soc.*, 2025, **147**, 17926–17935.
101 W. Park, Y. Reo, W. Yang, H. Choi, S. Jeon, B. Lim, A. Liu, H. Zhu and Y.-Y. Noh, Two-Dimensional Dion-Jacobson Tin Perovskite Transistors with Enhanced Ambient Stability, *ACS Energy Lett.*, 2024, **9**, 2436–2445.
102 L. Dou, A. B. Wong, Y. Yu, M. Lai, N. Kornienko, S. W. Eaton, A. Fu, C. G. Bischak, J. Ma, T. Ding, N. S. Ginsberg, L.-W. Wang, A. P. Alivisatos and P. Yang, Atomically Thin Two-Dimensional Organic-Inorganic Hybrid Perovskites, *Science*, 2015, **349**, 1518–1521.
103 Z. Tan, Y. Wu, H. Hong, J. Yin, J. Zhang, L. Lin, M. Wang, X. Sun, L. Sun, Y. Huang, K. Liu, Z. Liu and H. Peng, Two-Dimensional $(C_4H_9NH_3)_2PbBr_4$ perovskite Crystals for High-Performance Photodetector, *J. Am. Chem. Soc.*, 2016, **138**, 16612–16615.
104 T. Matsushima, M. R. Leyden, T. Fujihara, C. Qin, A. S. D. Sandanayaka and C. Adachi, Large Metal Halide Perovskite Crystals for Field-Effect Transistor Applications, *Appl. Phys. Lett.*, 2019, **115**, 120601.
105 L. Zhao, H. Tian, S. H. Silver, A. Kahn, T.-L. Ren and B. P. Rand, Ultrasensitive Heterojunctions of Graphene and 2D Perovskites Reveal Spontaneous Iodide Loss, *Joule*, 2018, **2**, 2133–2144.
106 Y. Reo, H. Zhu, J.-Y. Go, K. I. Shim, A. Liu, T. Zou, H. Jung, H. Kim, J. Hong, J. W. Han and Y.-Y. Noh, Effect of Monovalent Metal Iodide Additives on the Optoelectric Properties of Two-Dimensional Sn-Based Perovskite Films, *Chem. Mater.*, 2021, **33**, 2498–2505.
107 J.-Y. Go, H. Zhu, Y. Reo, H. Kim, A. Liu and Y.-Y. Noh, Sodium Incorporation for Enhanced Performance of Two-Dimensional Sn-Based Perovskite Transistors, *ACS Appl. Mater. Interfaces*, 2022, **14**, 9363–9367.
108 G. Park, W. Yang, A. Liu, H. Zhu, F. De Angelis and Y. Y. Noh, High-Performance Tin Perovskite Transistors through Formate Pseudohalide Engineering, *Mater. Sci. Eng., R*, 2024, **159**, 100806.
109 Y. Liu, P.-A. Chen, X. Qiu, J. Guo, J. Xia, H. Wei, H. Xie, S. Hou, M. He, X. Wang, Z. Zeng, L. Jiang, L. Liao and Y. Hu, Doping of Sn-Based Two-Dimensional Perovskite Semiconductor for High-Performance Field-Effect Transistors and Thermoelectric Devices, *iScience*, 2022, **25**, 104109.
110 J.-Y. Go, G. Byeon, T. Choi, S. Yang, W. Li and Y.-Y. Noh, A Large Bandgap Organic Salt Dopant for Sn-Based Perovskite Thin-Film Transistor, *Adv. Funct. Mater.*, 2023, **33**, 2303759.
111 R. N. Bukke, O. A. Syzgantseva, M. A. Syzgantseva, K. Aidinis, A. Soultati, A. Verykios, M. Tountas, V. Psycharis, T. Alshahrani, H. Ullah, L. P. Zorba, G. C. Vougioukalakis, J. Wang, X. Bao, J. Jang, M. K. Nazeeruddin, M. Vasilopoulou and A. R. B. Mohd Yusoff, Strain Relaxation and Multidentate Anchoring in N-Type Perovskite Transistors and Logic Circuits, *Nat. Electron.*, 2024, **7**, 444–453.
112 X.-J. She, C. Chen, G. Divitini, B. Zhao, Y. Li, J. Wang, J. F. Orri, L. Cui, W. Xu, J. Peng, S. Wang, A. Sadhanala and H. Sirringhaus, A Solvent-Based Surface Cleaning and Passivation Technique for Suppressing Ionic Defects in High-Mobility Perovskite Field-Effect Transistors, *Nat. Electron.*, 2020, **3**, 694–703.
113 T. Matsushima, S. Terakawa, M. R. Leyden, T. Fujihara, C. Qin and C. Adachi, Toward Air-Stable Field-Effect Transistors with a Tin Iodide-Based Hybrid Perovskite Semiconductor, *J. Appl. Phys.*, 2019, **125**, 235501.
114 J. Liu, H. Yao, S. Wang, C. Wu, L. Ding and F. Hao, Origins and Suppression of Sn(II)/Sn(IV) Oxidation in Tin Halide Perovskite Solar Cells, *Adv. Energy Mater.*, 2023, **13**, 2300696.
115 L. Lanzetta, T. Webb, N. Zibouche, X. Liang, D. Ding, G. Min, R. J. E. Westbrook, B. Gaggio, T. J. Macdonald, M. S. Islam and S. A. Haque, Degradation Mechanism of Hybrid Tin-Based Perovskite Solar Cells and the Critical Role of Tin (IV) Iodide, *Nat. Commun.*, 2021, **12**, 2853.
116 M. Mativenga, J. Ji, N. T. T. Hoang and F. Haque, Ambient Air Stability of Hybrid Perovskite Thin-Film Transistors by Ambient Air Processing, *Adv. Mater. Interfaces*, 2020, **7**, 1901777.
117 Y. Kim, J. Woo, Y.-K. Jung, H. Ahn, I. Kim, Y. Reo, H. Lim, C. Lee, J. Lee, Y. Kim, H. Choi, M.-H. Lee, J. Lee, S. D. Stranks, H. Sirringhaus, Y.-Y. Noh, K. Kang and T. Lee, Reversible Oxidative P-Doping in 2D Tin Halide Perovskite Field-Effect Transistors, *ACS Energy Lett.*, 2024, **9**, 1725–1734.
118 F. Zhang, Q. Zhang, X. Liu, Y. Hu, Z. Lou, Y. Hou and F. Teng, Property Modulation of Two-Dimensional Lead-Free Perovskite Thin Films by Aromatic Polymer Additives for Performance Enhancement of Field-Effect Transistors, *ACS Appl. Mater. Interfaces*, 2021, **13**, 24272–24284.
119 D. Han, J. Wang, L. Agosta, Z. Zang, B. Zhao, L. Kong, H. Lu, I. Mosquera-Lois, V. Carnevali, J. Dong, J. Zhou, H. Ji, L. Pfeifer, S. M. Zakeeruddin, Y. Yang, B. Wu, U. Rothlisberger, X. Yang, M. Gratzel and N. Wang, Tautomeric Mixture Coordination Enables Efficient Lead-Free Perovskite Leds, *Nature*, 2023, **622**, 493–498.
120 D. Yu, M. Pan, G. Liu, X. Jiang, X. Wen, W. Li, S. Chen, W. Zhou, H. Wang, Y. Lu, M. Ma, Z. Zang, P. Cheng, Q. Ji,

F. Zheng and Z. Ning, Electron-Withdrawing Organic Ligand for High-Efficiency All-Perovskite Tandem Solar Cells, *Nat. Energy*, 2024, **9**, 298–307.

121 S. Wang, K. Bidinakis, C. Haese, F. H. H. Hasenburg, O. Yildiz, Z. Ling, S. Frisch, M. Kivala, R. Graf, P. W. M. Blom, S. A. L. Weber, W. Pisula and T. Marszalek, Modification of Two-Dimensional Tin-Based Perovskites by Pentanoic Acid for Improved Performance of Field-Effect Transistors, *Small*, 2023, **19**, 2207426.

122 M. Xia, Z. Song, H. Wu, X. Du, X. He, J. Pang, H. Luo, L. Jin, G. Li, G. Niu and J. Tang, Compact and Large-Area Perovskite Films Achieved Via Soft-Pressing and Multi-Functional Polymerizable Binder for Flat-Panel X-Ray Imager, *Adv. Funct. Mater.*, 2022, **32**, 2110729.

123 V. Nketia-Yawson, B. Nketia-Yawson and J. W. Jo, Interfacial Interaction Enables Enhanced Mobility in Hybrid Perovskite-Conjugated Polymer Transistors with High-K Fluorinated Polymer Dielectrics, *Macromol. Rapid Commun.*, 2023, **44**, 2200954.

124 V. Nketia-Yawson, B. Nketia-Yawson, H. Opoku, J. H. Lee and J. W. Jo, Electrolyte-Gated Perovskite Transistors Functionalized with Conjugated Polymers, *ACS Mater. Lett.*, 2023, **5**, 388–396.

125 L. Zhu, H. Zhang, Q. Lu, Y. Wang, Z. Deng, Y. Hu, Z. Lou, Q. Cui, Y. Hou and F. Teng, Synthesis of Ultrathin Two-Dimensional Organic-Inorganic Hybrid Perovskite Nanosheets for Polymer Field-Effect Transistors, *J. Mater. Chem. C*, 2018, **6**, 3945–3950.

126 H. Zhu, A. Liu, H. L. Luque, H. Sun, D. Ji and Y.-Y. Noh, Perovskite and Conjugated Polymer Wrapped Semiconducting Carbon Nanotube Hybrid Films for High-Performance Transistors and Phototransistors, *ACS Nano*, 2019, **13**, 3971–3981.

127 Y. Kim and B. Park, Understanding Charge Trapping/Detrapping at the Zinc Oxide (ZnO)/$MAPbI_3$ Perovskite Interface in the Dark and under Illumination Using a ZnO/Perovskite/ZnO Test Platform, *Nanoscale*, 2018, **10**, 20377–20383.

128 D. Gedamu, I. M. Asuo, D. Benetti, M. Basti, I. Ka, S. G. Cloutier, F. Rosei and R. Nechache, Solvent-Antisolvent Ambient Processed Large Grain Size Perovskite Thin Films for High-Performance Solar Cells, *Sci. Rep.*, 2018, **8**, 12885.

129 H. Zhu, A. Liu, H. Kim, J. Hong, J.-Y. Go and Y.-Y. Noh, High-Performance Layered Perovskite Transistors and Phototransistors by Binary Solvent Engineering, *Chem. Mater.*, 2021, **33**, 1174–1181.

130 S. Wang, S. Frisch, H. Zhang, O. Yildiz, M. Mandal, N. Ugur, B. Jeong, C. Ramanan, D. Andrienko, H. I. Wang, M. Bonn, P. W. M. Blom, M. Kivala, W. Pisula and T. Marszalek, Grain Engineering for Improved Charge Carrier Transport in Two-Dimensional Lead-Free Perovskite Field-Effect Transistors, *Mater. Horiz.*, 2022, **9**, 2633–2643.

131 Z. Zhou, N. Guo, Y. Peng, L. Tang, J. Zhang, H. Cai, J. Ni, Y. Sun and J. Li, The Effect of Annealing Pressure on Perovskite Films and Its Thin-Film Field-Effect Transistors' Performance, *Phys. Status Solidi A*, 2019, **216**, 1900434.

132 C. Ma, S. Clark, Z. Liu, L. Liang, Y. Firdaus, R. Tao, A. Han, X. Liu, L. J. Li, T. D. Anthopoulos, M. C. Hersam and T. Wu, Solution-Processed Mixed-Dimensional Hybrid Perovskite/Carbon Nanotube Electronics, *ACS Nano*, 2020, **14**, 3969–3979.

133 S. Shao, W. Talsma, M. Pitaro, J. Dong, S. Kahmann, A. J. Rommens, G. Portale and M. A. Loi, Field-Effect Transistors Based on Formamidinium Tin Triiodide Perovskite, *Adv. Funct. Mater.*, 2021, **31**, 2008478.

134 W. Yang, G. Park, A. Liu, H. B. Lee, J.-W. Kang, H. Zhu and Y.-Y. Noh, Fluorinated Organic A-Cation Enabling High-Performance Hysteresis-Free 2D/3D Hybrid Tin Perovskite Transistors, *Adv. Funct. Mater.*, 2023, **33**, 2303309.

135 H. Zhu, W. Yang, Y. Reo, G. Zheng, S. Bai, A. Liu and Y.-Y. Noh, Tin Perovskite Transistors and Complementary Circuits Based on a-Site Cation Engineering, *Nat. Electron.*, 2023, **6**, 650–657.

136 H. Zhu, A. Liu, K. I. Shim, J. Hong, J. W. Han and Y.-Y. Noh, High-Performance and Reliable Lead-Free Layered-Perovskite Transistors, *Adv. Mater.*, 2020, **32**, 2002717.

137 I. H. Chao, Y.-T. Yang, M.-H. Yu, C.-H. Chen, C.-H. Liao, B.-H. Lin, I. C. Ni, W.-C. Chen, A. W. Y. Ho-Baillie and C.-C. Chueh, Performance Enhancement of Lead-Free 2D Tin Halide Perovskite Transistors by Surface Passivation and Its Impact on Non-Volatile Photomemory Characteristics, *Small*, 2023, **19**, 2207734.

138 F. Haque, H. Nhu Thi To, J. Ji and M. Mativenga, Effect of Precursor Composition on Ion Migration in Hybrid Perovskite $CH_3NH_3PbI_3$, *IEEE Electron Device Lett.*, 2019, **40**, 1756–1759.

139 H. Zhu, A. Liu, T. Zou, H. Jung, S. Heo and Y. Y. Noh, A Lewis Base and Boundary Passivation Bifunctional Additive for High Performance Lead-Free Layered-Perovskite Transistors and Phototransistors, *Mater. Today Energy*, 2021, **21**, 100722.

140 S. Jana, E. Carlos, S. Panigrahi, R. Martins and E. Fortunato, Toward Stable Solution-Processed High-Mobility P-Type Thin Film Transistors Based on Halide Perovskites, *ACS Nano*, 2020, **14**, 14790–14797.

141 H. Zhu, Y. Reo, G. Park, W. Yang, A. Liu and Y.-Y. Noh, Fabrication of High-Performance Tin Halide Perovskite Thin-Film Transistors Via Chemical Solution-Based Composition Engineering, *Nat. Protoc.*, 2025, **20**, 1915–1929.

142 J. Euvrard, Y. Yan and D. B. Mitzi, Electrical Doping in Halide Perovskites, *Nat. Rev. Mater.*, 2021, **6**, 531–549.

143 Y. Wang, Y. Cheng, C. Yin, J. Zhang, J. You, J. Wang, J. Wang and J. Zhang, Manipulating Crystal Growth and Secondary Phase PbI_2 to Enable Efficient and Stable Perovskite Solar Cells with Natural Additives, *Nano-Micro Lett.*, 2024, **16**, 183.

144 B. Jin, L. Ren, Y. Gou, R. Ma, Z. Liang, Z. Li, B. Dong, L. Zhao, S. Wang and C. Wu, Fiber-Bridging-Induced Toughening of Perovskite for Resistance to Crack Propagation, *Matter*, 2023, **6**, 1622–1638.

145 B. Xiao, Y. Qian, X. Li, Y. Tao, Z. Yi, Q. Jiang, Y. Luo and J. Yang, Enhancing the Stability of Planar Perovskite Solar Cells by Green and Inexpensive Cellulose Acetate Butyrate, *J. Energy Chem.*, 2023, **76**, 259–265.

146 J. Gong, H. Yu, X. Zhou, H. Wei, M. Ma, H. Han, S. Zhang, Y. Ni, Y. Li and W. Xu, Lateral Artificial Synapses on Hybrid Perovskite Platelets with Modulated Neuroplasticity, *Adv. Funct. Mater.*, 2020, **30**, 2005413.

147 Z. T. Xu, D. B. Mitzi, C. D. Dimitrakopoulos and K. R. Maxcy, Semiconducting Perovskites $(2\text{-}XC_6H_4C_2H_4NH_3)_2SnI_4$ (X = F, Cl, Br): Steric Interaction between the Organic and Inorganic Layers, *Inorg. Chem.*, 2003, **42**, 2031–2039.

148 H. H. Choi, K. Cho, C. D. Frisbie, H. Sirringhaus and V. Podzorov, Critical Assessment of Charge Mobility Extraction in Fets, *Nat. Mater.*, 2018, **17**, 2–7.

149 H. Xie, P.-A. Chen, X. Qiu, Y. Liu, J. Xia, J. Guo, H. Wei, Z. Gong, J. Ding and Y. Hu, Mxene-Based Metal Halide Perovskite Vertical Field-Effect Transistors: Toward High Current-Density and High Photodetection Performance, *Appl. Phys. Lett.*, 2023, **122**, 153301.

150 K. Pei, M. Chen, Z. Zhou, H. Li and P. K. L. Chan, Overestimation of Carrier Mobility in Organic Thin Film Transistors Due to Unaccounted Fringe Currents, *ACS Appl. Electron. Mater.*, 2019, **1**, 379–388.

151 J. Xia, C. Gao, C. Peng, Y. Liu, P.-A. Chen, H. Wei, L. Jiang, L. Liao, H. Chen and Y. Hu, Multidimensional Deep Ultraviolet (Duv) Synapses Based on Organic/Perovskite Semiconductor Heterojunction Transistors for Antispoofing Facial Recognition Systems, *Nano Lett.*, 2024, **24**, 6673–6682.

